

# Obesity-associated improvements in metabolic profile through expansion of adipose tissue

Ja-Young Kim,<sup>1</sup> Esther van de Wall,<sup>2</sup> Mathieu Laplante,<sup>3</sup> Anthony Azzara,<sup>2</sup> Maria E. Trujillo,<sup>1</sup> Susanna M. Hofmann,<sup>4</sup> Todd Schraw,<sup>1</sup> Jorge L. Durand,<sup>5</sup> Hua Li,<sup>5</sup> Guangyu Li,<sup>6</sup> Linda A. Jelicks,<sup>5</sup> Mark F. Mehler,<sup>6</sup> David Y. Hui,<sup>4</sup> Yves Deshaies,<sup>3</sup> Gerald I. Shulman,<sup>7</sup> Gary J. Schwartz,<sup>2,6,8,9</sup> and Philipp E. Scherer<sup>10</sup>

<sup>1</sup>Department of Cell Biology and <sup>2</sup>Department of Medicine, Albert Einstein College of Medicine, New York, New York, USA.

<sup>3</sup>Department of Anatomy and Physiology, Laval University Hospital Centre Research Centre, Laval University School of Medicine, Quebec City, Quebec, Canada. <sup>4</sup>Department of Pathology, Genome Research Institute, University of Cincinnati, Cincinnati, Ohio, USA. <sup>5</sup>Department of Physiology and Biophysics and <sup>6</sup>Department of Neuroscience, Albert Einstein College of Medicine, New York, New York, USA. <sup>7</sup>Department of Internal Medicine and Department of Cellular and Molecular Physiology, Yale University School of Medicine, and Howard Hughes Medical Institute, New Haven, Connecticut, USA.

<sup>8</sup>Department of Molecular Pharmacology and <sup>9</sup>Diabetes Research and Training Center, Albert Einstein College of Medicine, New York, New York, USA.

<sup>10</sup>Touchstone Diabetes Center, Department of Internal Medicine, University of Texas Southwestern Medical Center, Dallas, Texas, USA.

**Excess caloric intake can lead to insulin resistance. The underlying reasons are complex but likely related to ectopic lipid deposition in nonadipose tissue. We hypothesized that the inability to appropriately expand subcutaneous adipose tissue may be an underlying reason for insulin resistance and  $\beta$  cell failure. Mice lacking leptin while overexpressing adiponectin showed normalized glucose and insulin levels and dramatically improved glucose as well as positively affected serum triglyceride levels. Therefore, modestly increasing the levels of circulating full-length adiponectin completely rescued the diabetic phenotype in *ob/ob* mice. They displayed increased expression of PPAR $\gamma$  target genes and a reduction in macrophage infiltration in adipose tissue and systemic inflammation. As a result, the transgenic mice were morbidly obese, with significantly higher levels of adipose tissue than their *ob/ob* littermates, leading to an interesting dichotomy of increased fat mass associated with improvement in insulin sensitivity. Based on these data, we propose that adiponectin acts as a peripheral “starvation” signal promoting the storage of triglycerides preferentially in adipose tissue. As a consequence, reduced triglyceride levels in the liver and muscle convey improved systemic insulin sensitivity. These mice therefore represent what we believe is a novel model of morbid obesity associated with an improved metabolic profile.**

## Introduction

Adipose tissue plays a central role in the management of systemic energy stores as well as in many other processes (1). This is in part due to its capacity to store triglycerides but is also a function of its ability to secrete many proteins that have a major impact on energy homeostasis. A dysregulation of both processes leads to profound changes in insulin sensitivity at the level of the whole organism. Mice lacking specific adipocyte-derived secretory proteins, such as leptin, adiponectin, and resistin have metabolic phenotypes. On the other hand, mice lacking adipocytes altogether also display profound changes. Studies of several lipoatrophic models have been published (2–4). A common observation regarding many of these lipoatrophic or lipodystrophic models is that in the absence of functional adipocytes, triglycerides tend to be stored ectopically

in liver and muscle. These lipids, particularly as they relate to lipids in the liver, have been closely linked to insulin resistance (5).

This raises an interesting question. If accumulation of lipids in the liver and muscle were a “spillover” effect from adipose tissue, would it be possible to prevent this ectopic lipid accumulation if we enabled adipose tissue to expand beyond the limits observed under normal physiological conditions? We tested this in the context of *ob/ob* mice. The absence of leptin induced a massive hyperphagia and reduced energy expenditure, which are associated with a decrease in circulating adiponectin, a phenomenon shared by most obese, insulin-resistant models. The mice displayed dyslipidemia, hyperglycemia, and hyperinsulinemia. They accumulated large amounts of triglycerides in adipose tissue and are as a result among the most obese mouse models available to date. Despite massive obesity, the mice displayed a significant accumulation of hepatic triglycerides relatively early in life. This was an ideal setting to establish conditions that would allow adipose tissue to expand further. We found that overexpression of a mutated version of the adipokine adiponectin led to a significant increase in circulating levels of WT adiponectin protein as well as to an increase in adipocyte cell number and hence to an overall expansion of adipose tissue mass. Surprisingly, the uninhibited expansion of adipose tissue led to a complete normalization of all metabolic parameters tested despite the morbid obesity.

**Nonstandard abbreviations used:** aP2, adipocyte/macrophage fatty-acid-binding protein; CCR2, C-C motif chemokine receptor-2; DAG, diacylglycerol; 2DG, 2-deoxyglucose; DGAT-1, DAG acyltransferase; FPLC, fast-performance liquid chromatography; G-6-P, glucose-6-phosphate; GDI, GDP dissociation inhibitor; GDP, guanosine diphosphate; LPL, lipoprotein lipase; OGTT, oral glucose tolerance test; PEPCK, phosphoenolpyruvate carboxykinase; qRT-PCR, quantitative RT-PCR; RER, respiratory exchange ratio; SVC, stromal vascular cell; VO<sub>2</sub>, oxygen volume per time; WAT, white adipose tissue.

**Conflict of interest:** The authors have declared that no conflict of interest exists.

**Citation for this article:** *J. Clin. Invest.* 117:2621–2637 (2007). doi:10.1172/JCI31021.

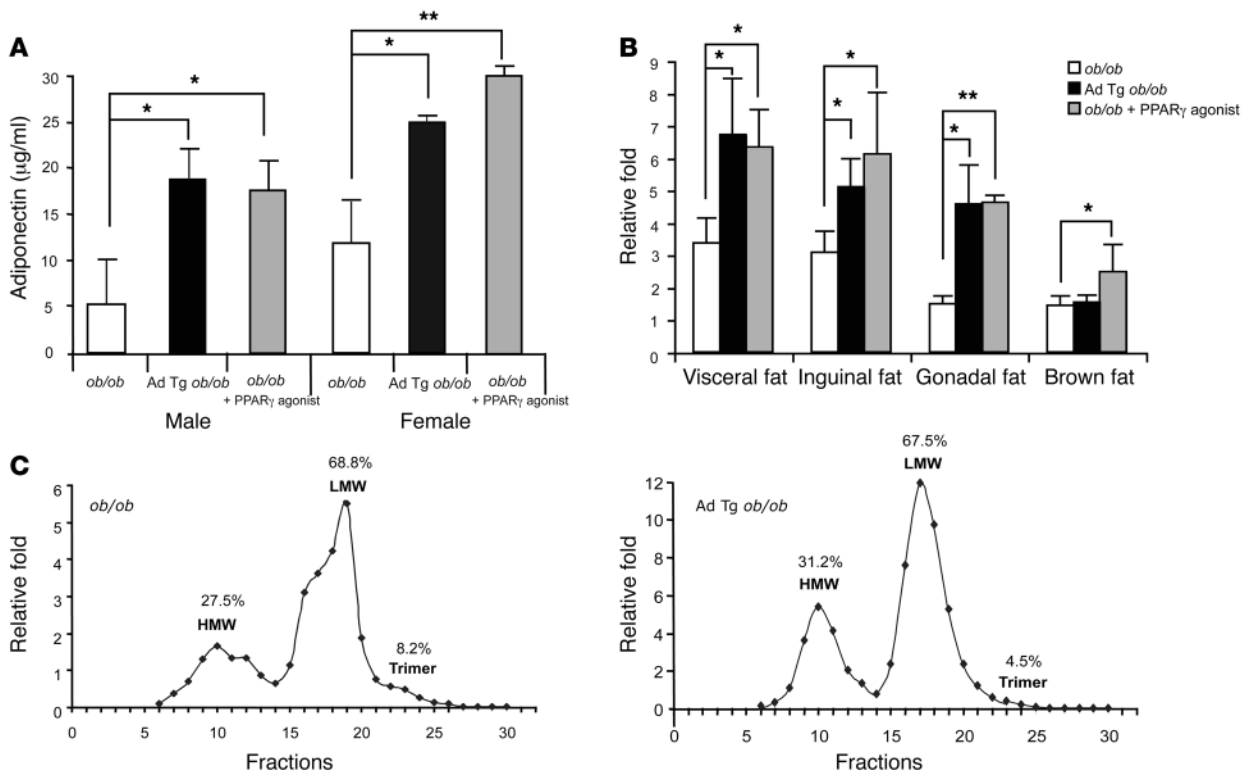


**Figure 1**  
*ob/ob* mice overexpressing adiponectin display physiological overexpression of adiponectin in circulation with normal adiponectin complex distribution. **(A)** Circulating adiponectin levels were measured by RIA in 12-week-old adiponectin transgenic *ob/ob* mice (Ad Tg *ob/ob*), their *ob/ob* littermates, and *ob/ob* mice with PPAR $\gamma$  agonist treatment ( $n = 5$  mice/group). **(B)** Tissue levels of adiponectin were measured in various fat pads, determined by Western blot analysis, and normalized with GDI in 12-week-old male adiponectin transgenic *ob/ob* mice, their *ob/ob* littermates, and *ob/ob* mice with PPAR $\gamma$  agonist treatment ( $n = 5$  mice/group). **(C)** The complex distribution of adiponectin of female mice was determined using gel filtration chromatography of serum samples followed by Western blot analysis of adiponectin in different fractions. A representative sample is shown. HMW, high molecular weight form; LMW, low molecular weight form (hexamer). \* $P < 0.05$ ; \*\* $P < 0.01$  by Student's  $t$  test.

While many mouse models with defects in proper adipose tissue development have been described, we believe this is the first genetically engineered model that directly highlights that fat mass expansion has potent antidiabetic effects. These observations fully support the data obtained in pharmacological models in which an effective expansion of fat mass can be encountered, such as in the context of the PPAR $\gamma$  agonists, the thiazolidinediones. They suggest that one of the key factors that link excess caloric intake and a positive energy balance with insulin resistance and type 2 diabetes is the inability to appropriately expand the (subcutaneous) adipose tissue. With respect to adiponectin physiology, they suggest that adiponectin serves as a starvation signal released by the adipocyte, indicating a local need to further expand triglyceride stores in adipose tissue. As a result, triglycerides were effectively redistributed from hepatocytes and muscle cells to subcutaneous adipose tissue. This redistribution coupled to increased adipogenesis resulted in the expected improvements in all the metabolic parameters, including a reduction in a number of proinflammatory factors.

**Results**

*Transgenic ob/ob mice overexpress adiponectin at levels comparable to those obtained by PPAR $\gamma$  agonist treatment.* To determine the consequences of a moderate overexpression of full-length adiponectin

in *ob/ob* mice, we used a transgenic cassette that we have previously described (6). This triggered an effective increase of steady state concentrations of adiponectin in plasma about 2- to 3-fold above baseline. This increase was comparable to the levels that can be obtained in *ob/ob* mice upon exposure to PPAR $\gamma$  agonists (Figure 1A). Similarly, tissue-associated adiponectin levels were also increased at a comparable degree in a number of different fat pads, except in brown adipose tissue (Figure 1B). This represented a relatively modest overexpression of adiponectin, well within the physiological range (7). Since adiponectin circulates in several different forms in plasma, we measured the relative abundance of the different complexes by gel filtration analysis, a method that efficiently separates high molecular weight, hexameric, and trimeric complexes. The transgenic mice carried all 3 complexes in circulation, albeit with a slight bias toward higher HMW forms compared with *ob/ob* mice (Figure 1C). We conclude therefore that this is a model of modest overexpression of adiponectin with properly assembled complexes in circulation.

*Modest adiponectin overproduction results in dramatic improvements in the baseline values of metabolic parameters of ob/ob mice.* To determine whether this modest overexpression of adiponectin has an impact on any of the metabolic parameters dysregulated in *ob/ob* mice, we determined fasting glucose, insulin, triglyceride, and FFA levels (Table 1). All parameters measured showed dramatic



**Table 1**  
Fasting serum parameters for WT, *ob/ob*, and transgenic *ob/ob* mice

	WT	<i>ob/ob</i>	Ad Tg <i>ob/ob</i>
Glucose (mg/dl)	92.4 ± 11.6 <sup>A</sup>	313.8 ± 76.6	100.6 ± 8.5 <sup>A</sup>
Insulin (ng/ml)	1.83 ± 0.51 <sup>B</sup>	7.85 ± 1.02	2.33 ± 0.53 <sup>B</sup>
Triglycerides (mg/dl)	147.2 ± 27.34 <sup>B</sup>	300.37 ± 114.2	93.5 ± 34.5 <sup>A</sup>
FFA (mmol/l)	2.05 ± 0.93	3.13 ± 0.13	2.56 ± 0.46

Data obtained from 8-week-old male animals. Values significantly differing from the *ob/ob* mice are indicated with a footnote. <sup>A</sup>*P* < 0.01; <sup>B</sup>*P* < 0.05. Ad Tg *ob/ob*, adiponectin transgenic *ob/ob* mice.

improvements, with glucose levels reaching near hypoglycemic levels, insulin levels significantly lowered, and a highly significant lowering of triglycerides and FFAs.

*Normalization of parameters during metabolic challenges.* We wanted to know whether these improvements in baseline values also translated into improvements upon exposing the mice to glucose and lipid challenges. During an oral glucose tolerance test (OGTT), the transgenic animals displayed a much more efficient clearance of systemic glucose levels than *ob/ob* littermates (Figure 2A). In addition, the transgenic animals had a much more robust glucose-induced insulin release during the OGTT compared with the hyperinsulinemic *ob/ob* littermates, which showed a much more delayed and less dramatic increase over baseline (Figure 2A). Upon exposure of the mice to an oral triglyceride gavage, *ob/ob* mice showed the expected high excursion/slow clearance of triglycerides from circulation. The increased levels of adiponectin levels effectively prevented circulating lipids from ever rising much above baseline. As there was no evidence for malabsorption of nutrients from the gut (data not shown), this suggests that the transgenic mice developed extremely efficient mechanisms for the removal of dietary fat from circulation (Figure 2B).

To determine whether an induced loss of function of adiponectin in the transgenics has an impact on the rate of lipid clearance, we treated the mice for 1 week with either a mixture of 2 monoclonal antibodies raised against adiponectin that effectively trigger a reduction in circulating adiponectin or with equal amounts of a nonimmune mouse IgG preparation (Figure 2C). The relatively sudden reduction in adiponectin levels led to a trend toward reduction in the clearance rate of the ingested triglycerides, suggesting that both acute and chronic differences mediated the metabolic differences between these 2 mouse models.

As an additional functional test for both adipocytes and  $\beta$  cells, we exposed the mice to an injection of the  $\beta 3$  adrenergic agonist CL-316,243. Exposure to CL-316,243 triggered a response that was critically dependent on the presence of the  $\beta 3$  adrenergic receptor in white adipose tissue (WAT) and resulted in a very acute, sharp rise in insulin secreted from pancreatic  $\beta$  cells (8). The underlying reasons for this phenomenon are not yet known, but fully functional WAT and functional  $\beta$  cells are required. CL-316,243 significantly stimulated lipolysis in both mouse models assessed by increased circulating FFAs after stimulation. While the baseline FFA values had a tendency to be lower in the transgenic mice,  $\beta 3$  agonist-mediated lipolysis was increased compared with that of *ob/ob* mice (Figure 2D). However, more dramatic differences became apparent when looking at  $\beta 3$  agonist-stimulated insulin release. Mice lacking leptin were hyperinsulinemic at baseline but

failed to further increase the insulin levels upon stimulation. The transgenic animals, in contrast, showed a robust increase in insulin release upon stimulation of  $\beta 3$  adrenergic receptors in WAT, suggesting full reconstitution of this process both at the level of WAT and at the level of pancreatic  $\beta$  cells (Figure 2D).

*Effects on lipoprotein particle distribution.* In light of the fairly dramatic effects seen on baseline triglyceride levels and during the oral triglyceride gavage, we wanted to see whether there were any changes in lipoprotein particle distribution. To that end, we size fractionated serum from the 2 strains by conventional size-exclusion chromatography and measured cholesterol and triglyceride distribution (Figure 2E). In addition to a reduction of total cholesterol levels in all particle fractions, there were also subtle but reproducible shifts toward a higher density within the cholesterol containing HDL particles. Adiponectin-overexpressing mice showed a marked decrease in the main HDL peak and in the shoulder, where HDL-1 and LDL elute, compared with the plain *ob/ob* background. The triglyceride levels associated with the particle fractions were so low in the transgenic animals that, with the exception of the VLDL fraction, triglyceride levels were below the detection limit in all particle fractions. The apoE content of HDL was reduced in adiponectin-overexpressing *ob/ob* mice compared with *ob/ob* mice, suggesting that adiponectin reduces the levels of apoE-enriched, cholesterol ester rich HDL-1 (Figure 2F). On the other hand, the apoA1 and A2 content of HDL were similar in both transgenic and nontransgenic mice (data not shown). This suggests that the increased levels of adiponectin may effectively overcome the established impairment in HDL turnover that normal *ob/ob* mice display (9).

*Transgenic mice are resistant to the deleterious impact of high-fat diets on insulin sensitivity.* Exposure to a high-fat diet for 6 weeks further exacerbated the effects on glucose and lipids. High-fat diet further impaired the metabolic state of *ob/ob* mice, yet adiponectin-overexpressing mice are resistant to this high-fat diet-induced deterioration of metabolic parameters. Glucose levels remained unchanged on the high-fat diet (Figure 2G), and OGTT did not show significant change in glucose clearance (Figure 2G), while *ob/ob* mice demonstrated a worsening of the clearance rate. Insulin levels remained low, and FFA levels did not change significantly either (Figure 2G).

In addition, we wanted to determine whether the ability to respond to a central hypoglycemic stimulus was preserved in the transgenic animals compared with *ob/ob* animals. We infused a bolus of 2-deoxyglucose (2DG) centrally i.c.v. This mimicked a systemic hypoglycemic response, prompting central compensatory mechanisms, triggering a number of peripheral responses and sending a strong vagal stimulus to the liver to initiate a gluconeogenic response (10). In WT animals, the resulting hyperglycemia triggered the expected compensatory reduction of hepatic glucose output, leading to a rapid normalization of plasma glucose levels. While *ob/ob* mice displayed a very significant initial excursion of glucose levels, they failed to appropriately compensate for hepatic glucose output and remained hyperglycemic throughout the rest of the time course. The transgenic animals, however, displayed a response comparable to that of WT mice, further highlighting the improvements in hepatic carbohydrate metabolism (Figure 2H).

*The metabolic improvements are associated with an increase in adipose tissue mass.* A systematic analysis of the age-dependent weight gain revealed that *ob/ob* animals with increased adiponectin levels displayed markedly higher body weights than their *ob/ob* counter-

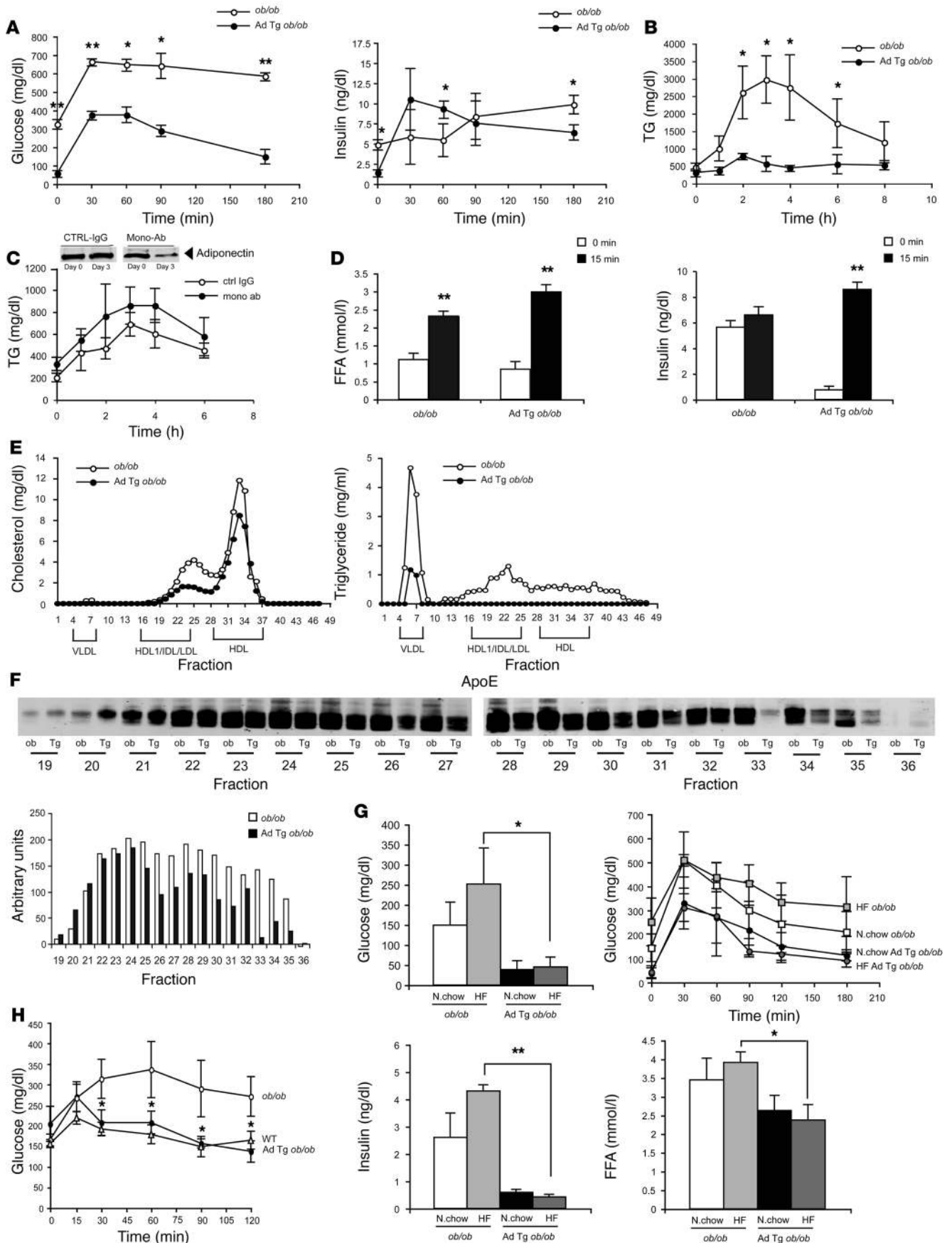




## Figure 2

Adiponectin improves the metabolic profile of *ob/ob* mice. (A) Circulating glucose and insulin levels measured during OGTT. (B) Plasma triglyceride (TG) levels measured during lipid challenge in adiponectin transgenic *ob/ob* mice and their *ob/ob* littermates. (C) Plasma triglyceride levels were measured during a lipid challenge in adiponectin transgenic *ob/ob* mice after an injection of 2 monoclonal anti-adiponectin antibodies (Mono-Ab) or control mouse IgGs (CTRL-IgG). (D) Plasma insulin (right) and FFA levels (left) monitored after i.p. CL-316,243 injection in adiponectin transgenic *ob/ob* mice and their *ob/ob* littermates. (E) Cholesterol and triglyceride levels were measured in plasma samples subfractionated by gel filtration chromatography. LDL, intermediate density lipoprotein. (F) apoE levels were measured in the same fractions by Western blot analysis (top) and quantitated (bottom). (G) Adiponectin transgenic *ob/ob* mice and their *ob/ob* littermates were fed normal chow (N chow) or high-fat diet (HF) for 6 weeks. Fasting glucose levels (top left), glucose levels during an OGTT (top right), insulin levels (bottom left), and FFA levels (bottom right) were determined in adiponectin transgenic *ob/ob* mice and their *ob/ob* littermates (A–G,  $n = 5$  mice/group). (H) 2DG was centrally delivered to adiponectin transgenic *ob/ob* mice, *ob/ob* littermates, and WT mice, and blood glucose levels were monitored during indicated times ( $n = 3$  mice/group). Experiments were performed with 10- to 12-week-old adiponectin transgenic *ob/ob* mice, *ob/ob* littermates, and WT male mice. \* $P < 0.05$ ; \*\* $P < 0.01$ . Panels A and B were analyzed by ANOVA; panels D and G were analyzed by Student's *t* test.

parts, the current gold standard for obesity in mice (Figure 3A). As these mice aged, the average weight difference was more than 30 grams. A representative example of 2 male siblings, one with, the other one without transgene is shown.

Body composition analysis performed with an EchoMRI revealed that all of the extra body weight could be accounted for by an increase in adipose tissue mass (Figure 3B). Due to the size restrictions for the conventional EchoMRI machines, only young animals could be measured for body composition. The absolute weight contributions of the 3 different compartments that can be distinguished by EchoMRI are indicated, referring to lean body mass, fat mass that includes adipose tissue, and contributions of other compartments, such as bone. The weight differences became more extreme when the mice were exposed to a high-fat diet (Figure 3C). The transgenic mice showed a significant increase in fat mass while preserving euglycemia (Figure 2G). A histological examination of various adipose tissue pads revealed remarkable differences with respect to average adipocyte size. The fat from *ob/ob* mice displayed the expected enlarged, lipid-engorged adipocytes. Adipose tissue from transgenic animals, in contrast, displayed a larger number of adipocytes with much smaller average cell size in gonadal fat pads (Figure 3D). Similar observations can be made for other fat pads, such as subcutaneous fat (data not shown). A representative picture of gonadal adipose tissue is shown in Figure 3E. Quantification of average cell area in a number of representative histological sections (Figure 3D) further highlighted the significant size difference. In light of the overall increase in adipose tissue mass, this suggests that the transgenic mice displayed a significant hyperproliferation of adipocytes.

**Normalization of islet size and reduction of liver triglyceride and diacylglycerol content.** To test whether the improvements in systemic insulin sensitivity are also associated with improvements at the level of the  $\beta$  cell, we examined a large number of pancreatic sections histologically. The average islet diameter was considerably reduced compared with the classical hypertrophic phenotype seen in the islets of *ob/ob* mice (judged both histologically and quantitatively), and the overall integrity of the islets was much better preserved (Figure 3E).

The *ob/ob* mice displayed a propensity to accumulate triglycerides in the liver, a phenomenon that is likely to contribute to the reduced systemic insulin sensitivity. Liver sections from *ob/ob* animals displayed a clearly visible positive signal for oil red O, a stain highlighting neutral lipids in tissues (Figure 3F). There was a marked reduction in the lipid stain in the transgenic animals. Measurements of total liver triglycerides confirmed the visual impression, highlighting the marked decrease in hepatic steatosis

(Figure 3F). This was further corroborated with measurements of one of the key metabolites, diacylglycerol (DAG), in the liver. DAG can activate a number of PKC isoforms, some of which have been implicated as inhibitors of insulin signaling. Specifically, activation of DAG-sensitive PKC isoforms that include PKC- $\theta$  in skeletal muscle (11) and PKC- $\epsilon$  in the liver (12–14) downregulates insulin receptor signaling and may represent a biochemical link between dysregulated lipid metabolism and insulin resistance. DAG levels were indeed reduced in transgenic animals (Figure 3F), lending further support for the presence of an excellent hepatic metabolic profile despite a high degree of adiposity.

**Subcutaneous, but not intraabdominal, fat pads increase in size.** Upon dissection of the animals, it was quite apparent that the visceral fat pads in the transgenic animals matched more closely those found in WT animals than those of their obese littermates (Figure 3G) while most other fat pads displayed the expected increase in volume (data not shown). The increase in overall adiposity was therefore primarily due to increases in nonvisceral depots, i.e., subcutaneous adipose tissue. One notable exception was the pericardial fat, which was disproportionately increased in the transgenic mice as well, leading to a 5-fold increase in total pericardial fat mass. A representative pair of pericardial fat pads is shown in a 3D reconstruction (Figure 3H). Of note is also the observation that the heart volume of the transgenic animals was significantly larger (>30%) than that of *ob/ob* mice (not shown), suggesting that excess adiponectin leads to cardiomyopathy. Whether this is a specific consequence of excess adiponectin in circulation or the result of the overall increase in weight is not known to date. No weight differences were observed for other organs, such as the liver, and the increased heart weights can be observed even in transgenic animals on a WT background that do not display such a significant increase in overall fat mass (data not shown).

**Significant improvements in hepatic insulin sensitivity.** To determine whether hepatic insulin sensitivity improved in the transgenic mice, we performed an in vivo insulin sensitivity assay. Mice were fasted and injected with insulin, and livers were then extracted after the indicated time points. Analysis of the phosphorylation state of the insulin receptor and a number of downstream targets demonstrated a significant improvement in insulin sensitivity as judged by the increased phosphorylation state of these proteins upon insulin exposure (Figure 3I).

**Immunohistological analysis of islets and adipose tissue revealed dramatically improved islet histology.** To see whether the normalization of islet size also translated into a normalization of cell-type distribution, we performed an immunohistochemical analysis of islets (Figure 4A). Compared with islets from *ob/ob* mice, transgenic *ob/ob* mice displayed a

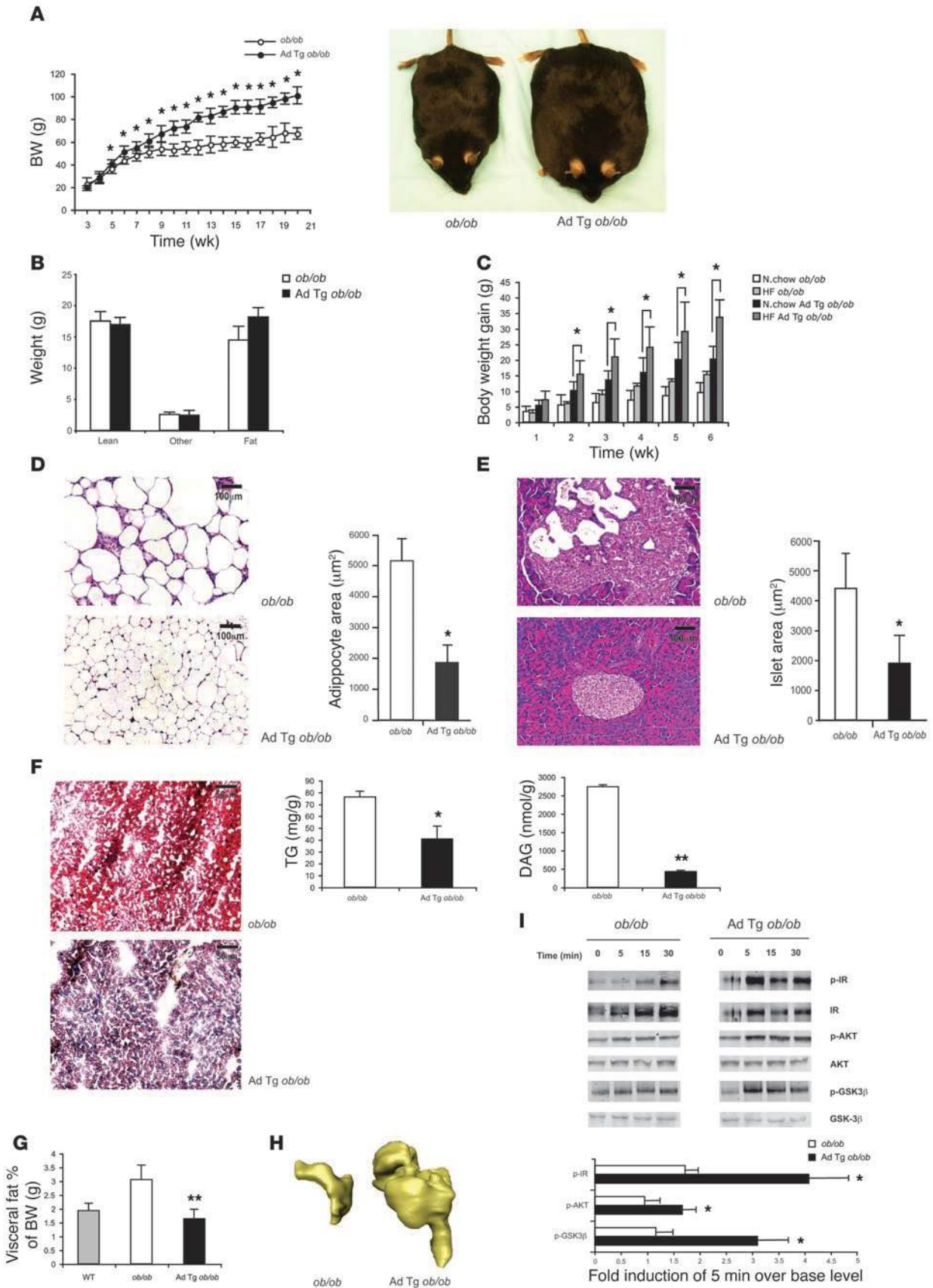




### Figure 3

*ob/ob* mice expressing adiponectin are heavier but healthier than *ob/ob* mice, displaying increased fat mass and decreased liver triglycerides. (A) Changes in body weight were monitored ( $n = 15$  mice/group). Representative animals are shown: an *ob/ob* mouse and an adiponectin transgenic *ob/ob* littermate at 12 weeks. (B) Body composition of 5-week-old mice was measured by MRI ( $n = 3$  mice/group). (C) Body weight gain was tracked on normal chow or on a HF diet in 10-week-old adiponectin transgenic *ob/ob* mice and *ob/ob* littermates. (D) Sections of gonadal WAT and (E) pancreatic islets from adiponectin transgenic *ob/ob* mice (top) and *ob/ob* littermates (bottom) were H&E stained. The average adiponectin size calculated (D, right panel) and surface area of >100 islets stained for insulin was measured and average islet area is indicated (E, right panel). (F) Frozen sections of liver from adiponectin transgenic *ob/ob* mice and *ob/ob* littermates were stained with oil red O (left panel). Liver triglyceride content (middle panel) and DAG levels (right panel) were analyzed. (G) Intraabdominal visceral fat pads from WT mice, adiponectin transgenic *ob/ob* mice, and *ob/ob* littermates were weighed and presented as percentage of total body weight (F and G,  $n = 4-5$  mice/group). (H) Pericardial fat pads from 10-week-old female mice were imaged by MRI and reconstituted into a 3D representation. A representative example is shown. (I) Mice were fasted for 6 hours and injected with 1 mU of insulin/g body weight. At indicated time points, 1 mouse was sacrificed and liver protein was extracted and analyzed for the total and phosphorylated forms of the indicated targets using 3 independent measurements for each time point. \* $P < 0.05$ ; \*\* $P < 0.01$ . Panels A and C were analyzed by ANOVA; panels D, F, G, and I were analyzed by Student's *t* test.

normalized distribution and staining intensity for  $\alpha$  cells (glucagon) and  $\beta$  cells (insulin). The immunohistological appearance of these islets was nearly identical to what can be observed in WT animals.

*Macrophage infiltration is not a function of fat mass.* It is well established that increased adiposity is associated with increased infiltration of macrophages into adipose tissue (15, 16). The transgenic model presented here offers an interesting opportunity to determine whether this is strictly a function of fat mass. Staining of WAT with antibodies to the macrophage marker F4/80 showed the expected high frequency of F4/80-positive cells in the *ob/ob* mice. Interestingly, despite the massive obesity in the transgenic *ob/ob* mice, it was difficult to detect any F4/80-positive cells in the WAT of these mice (Figure 4B). Due to the nonquantitative nature of immunohistochemistry, we complemented this data with FACS analysis to quantitate the number of macrophages in the fat pads isolated from the 2 mouse strains. This analysis confirmed the immunohistochemical data, as the number of macrophages was sharply reduced in the fat pad isolated from transgene-positive mice (Figure 4C). This was further confirmed by quantitative RT-PCR (qRT-PCR) for the message for the F4/80 surface marker (Figure 4C). In addition, we aimed to obtain a quantitative measurement of the degree of inflammation in the vascular endothelium in adipose tissue of these mice. We used vWF as a marker of the endothelium, which is relatively constitutively expressed, and VCAM-1 as an inflammation-sensitive readout. The ratio of VCAM-1 to vWF was therefore a valuable indicator of the local degree of inflammation in the endothelium. Figure 4D shows that this ratio between these 2 markers was significantly smaller in the transgenic animals. Therefore, a statistically significant decrease was observed in the vasculature of transgenic adipose tissue with respect to the degree of inflammation. As we and others have demonstrated a significant impact of adipose tissue on systemic inflammation with respect to IL-6 levels, we predicted that in light of the reduced overall inflammation in adipose tissue, the systemic levels of IL-6 should also drop in the transgenic animals. As seen in Figure 4E, the circulating IL-6 levels were significantly reduced in the animals expressing increased levels of adiponectin. In addition, we also performed qRT-PCR analysis for TNF- $\alpha$  in adipose tissue, which was also reduced (Figure 4E).

*Changes underlying the altered metabolic phenotype in the transgenic mice.* To gain a better understanding of the underlying molecular changes that led to the improvements in the metabolic phenotype, we looked at a number of different parameters in adipose tissue and in plasma. Lipoprotein lipase (LPL) plays a key role in the clearance of circulating triglycerides and their routing toward storage or oxidative tis-

ues. LPL activity was elevated in several white fat pads of transgenic animals (Figure 5A). When expressed per whole depot, LPL in the expanded subcutaneous fat was increased more than 2-fold, and it was increased 5-fold in brown adipose tissue of transgenic compared with *ob/ob* littermates (not shown). Concomitantly, there was a marked elevation in heparin-releasable LPL in plasma, a reflection of the global intravascular availability of the enzyme. An overview of the expression levels of mRNAs encoding some relevant enzymes in lipid metabolism demonstrated increases in cytosolic phosphoenolpyruvate carboxykinase (PEPCK), diacylglycerol acyltransferase (DGAT-1), PPAR $\gamma$ 2, and adipocyte/macrophage fatty-acid-binding protein (aP2) in the adipose tissue (Figure 5B). LPL, PEPCK, DGAT-1, and aP2 are all well established PPAR $\gamma$  targets. To obtain a more comprehensive overview of gene expression in the adipose tissue of transgenic mice, a series of microarray experiments was performed. This global gene expression analysis with NimbleGen arrays revealed a large number of transcriptional changes in adipose tissue of transgenic mice. The general transcriptional fingerprint of this adipose tissue revealed an increase in lipogenesis along with an increase in the levels of mitochondrial genes and a reduction of pro-inflammatory markers (Supplemental Table 1; available online with this article; doi:10.1172/JCI31021DS1), consistent with reported changes upon PPAR $\gamma$  agonist treatment. Indeed, mRNA levels of PPAR $\gamma$ , PGC1 $\alpha,\beta$ , and RXR $\alpha$  were also increased. Importantly, the microarray data fully confirmed the data obtained independently by qPCR for PEPCK, DGAT-1, PPAR $\gamma$ 2, and aP2.

*Elevation of peripheral adiponectin reduces food intake and energy expenditure.* An important question is whether the massive accumulation of adipose tissue is the result of increased caloric intake or reduced energy expenditure or a combination of the two. Mice lacking leptin and their transgenic littermates ate approximately the same amount of food per gram of lean body mass when they were young or old (Figure 6A). Since the transgenic littermates were much heavier at a later age, this translates into a very significantly reduced amount of food intake per gram of body weight in the presence of the transgene (Figure 6A). In light of the net increase of body fat, this suggests that the transgenic mice were metabolically much more efficient. Consistent with that, the body core temperature was significantly lower in the transgenic animals at all ages, particularly during the dark cycle (Figure 6B). The essential finding is therefore that the transgenic mice had a food intake comparable to that of their *ob/ob* littermates. While we expected a higher energy expenditure in these heavier animals, the exact opposite occurred. This suggests that adiponectin over-expression results in a negative regulation of energy expenditure.

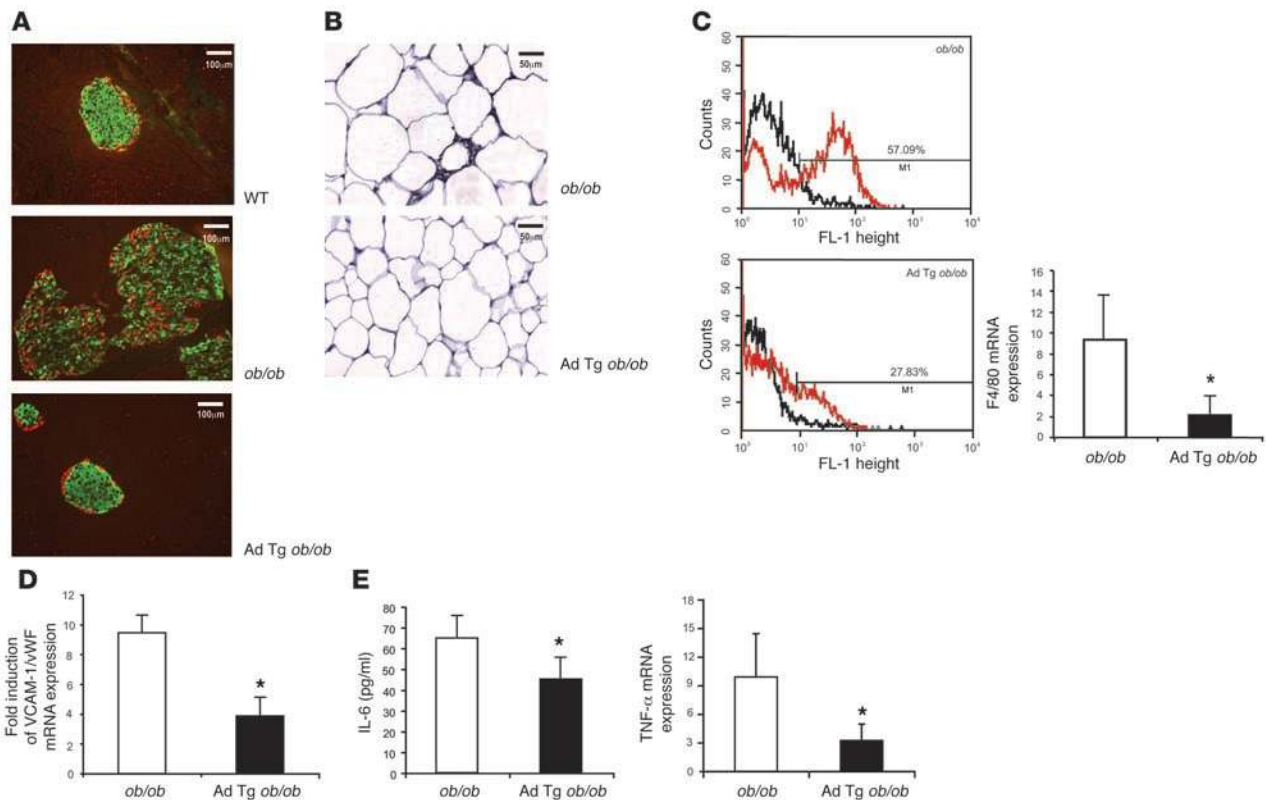


**Figure 4** Excess adiponectin normalizes pancreatic islet histology and improves both local and systemic inflammation. **(A)** Immunofluorescence staining for insulin (green) and glucagon (red) was performed in pancreatic sections from 10-week-old male WT mice (top), *ob/ob* littermates (middle), and adiponectin transgenic *ob/ob* mice. **(B)** Immunohistochemical staining of gonadal adipose tissue with anti-F4/80 antibodies suggests reduced infiltration of macrophages. Note that the difference in average adipocyte size between the 2 genotypes is apparent but less pronounced at this younger age. **(C)** FACS analysis of the stromal vascular fraction using F4/80 antibodies (left) and qRT-PCR for F4/80 (right) ( $n = 10$  mice/group) were performed in gonadal WAT of adiponectin transgenic *ob/ob* mice and *ob/ob* littermates. Black curve shows control IgG staining; red curve shows anti-F4/80 staining. **(D)** mRNA levels of vWF and VCAM-1 from WAT were measured by qRT-PCR. A ratio of VCAM-1/vWF is provided as an indicator of local inflammation in the vascular endothelium. **(E)** Circulating IL-6 was measured in adiponectin transgenic *ob/ob* mice and *ob/ob* littermates (top); adipose tissue TNF- $\alpha$  message levels (bottom). **(C–E)** For these studies, 14-week-old male mice were used ( $n = 10$  mice/group). \* $P < 0.05$ . Panels **C–E** were analyzed by Student’s *t* test.

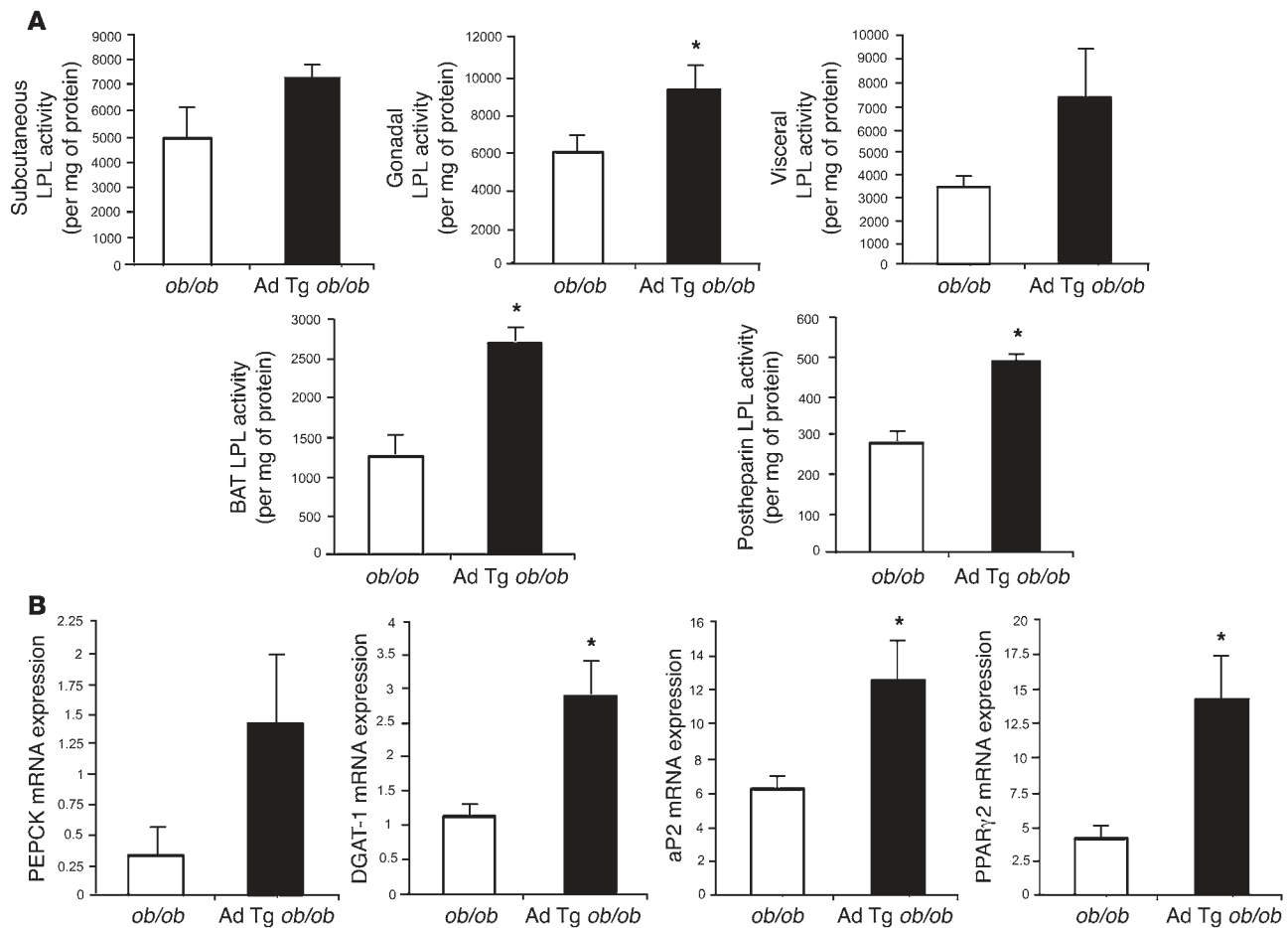
Unlike *ob/ob* animals, transgenic animals showed reductions in multiple behavioral and physiological measures relevant for determining overall energy balance, including body temperature, locomotor activity, and oxygen consumption. These reductions were characterized by a relative absence of typical diurnal rhythms. While lateral ambulatory and vertical rearing movement were not significantly different in younger animals (data not shown), older transgenic animals were significantly less active than age-matched *ob/ob* mice, again particularly during the dark cycle (Figure 6C). In light of the reduced caloric intake and increased fat mass, an overall improvement in metabolic efficiency would be expected. Energy expenditure was indeed reduced in the transgenic mice, accounting at least in part for the increased ability to store triglycerides in the context of reduced caloric intake. Oxygen consumption was reduced in the transgenic animals, as assessed by reduced oxygen volume per time ( $VO_2$ ), particularly during the dark cycle. (Figure 6D). No significant differences were seen between the 2 models at the level of the respiratory exchange ratio (RER) during free access to food (Figure 6E).

*Increasing adiponectin levels in the absence of leptin leads to starvation intolerance.* The very high tendency to store triglycerides in adipose

tissue raises the question of whether these lipid stores can appropriately be activated in times of need. In principle, the  $\beta_3$  adrenergic axis was intact in both mouse models with respect to induction of lipolysis (Figure 2D). However, it was not clear whether this translates into an equally efficient response to starvation. Preliminary experiments in the context of caloric restriction had demonstrated that the increased levels of adiponectin resulted in a decreased weight loss during caloric restriction (data not shown), suggesting that it may be more difficult for the transgenic mice to tap into lipid stores during times of reduced exogenous caloric intake.

RER values were not significantly different between the 2 mouse lines during free access to food. However, during an acute fast, RER dropped significantly faster in the transgenic mice, suggesting an increased dependence on fatty acid oxidation early on in the fast (Figure 6F). Nevertheless, both strains reached asymptotic respiratory quotient values characteristic of fat mobilization within 12 hours. Activity increased in both groups in response to fasting, but activity levels were lower overall in transgenic mice (Figure 6G). Furthermore, increases in circulating adiponectin seen in the transgenic mice cause the complete absence of any diurnal



**Figure 5**

Increased adiponectin in *ob/ob* mice triggers improvements in lipid metabolism. (A) LPL activity of 12-week-old mice was measured in a number of different fat pads as well as in plasma. ( $n = 5$  mice/group). (B) mRNA levels of PEPCK, DGAT-1, PPAR $\gamma$ 2, and aP2 were measured by qRT-PCR ( $n = 5$  mice/group) in WAT from 12-week-old adiponectin transgenic *ob/ob* mice and *ob/ob* littermates. \* $P < 0.05$ . Panels A and B were analyzed by Student's *t* test.

nal variability of glucose and FFAs, while *ob/ob* mice maintained a clear diurnal pattern (Figure 6H). Unlike fasted controls, fasted transgenic mice showed no diurnal variation in plasma glucose and FFA and overall had markedly reduced levels of these fuels relative to controls. However, the transgenic animals managed to sustain reasonable glucose and FFA levels at all times. Fasting  $VO_2$  and core temperature did not differ significantly between strains (Figure 7A), and fasting restored the diurnal fluctuations in both  $VO_2$  and core temperature in transgenic mice. In a separate experiment, we subjected cohorts of male and female mice to a 36-hour fast. We noticed that the fasted transgenic mice lost less weight than fasted *ob/ob* controls. This was a phenomenon seen in both females (Figure 7B) and males (data not shown), but the females showed a more pronounced difference. Similarly, the females had a more severe trend toward hypoglycemia during the fast (Figure 7C). In light of the lower plasma glucose levels in the transgenic animals throughout the fast, we wanted to test whether the livers from these animals displayed a reduced ability to induce gluconeogenesis. To do that, we looked at the message levels of PEPCK and glucose-6-phosphate (G-6-P). Changes in the message levels for these 2 enzymes are suggestive of changes in the gluconeogenic

pathway. While the males did not display a significant difference, the transgenic females had a significantly impaired ability of liver to mount a gluconeogenic response, consistent with the hypoglycemia observed throughout the fasting experiment (Figure 7D). The more striking effects in the females were consistent with the considerably higher adiponectin levels that could be achieved in females in this model (6).

## Discussion

To our knowledge, this is the first detailed analysis of a mouse model that directly supports the hypothesis that enabling a massive expansion of the subcutaneous adipose tissue mass potentially counteracts the strong trends toward the development of insulin resistance associated with excess caloric intake. We have chosen to address this issue in the *ob/ob* mouse model. These mice displayed hyperphagia and early onset obesity, resulting in hyperglycemia, hyperinsulinemia, and dyslipidemia. We achieved a normalization of all metabolic parameters through a modest overexpression of adiponectin. We were employing a transgene under the control of the fat cell-specific aP2 promoter that we previously characterized in the background of WT mice. This transgene encodes a version of adipon-

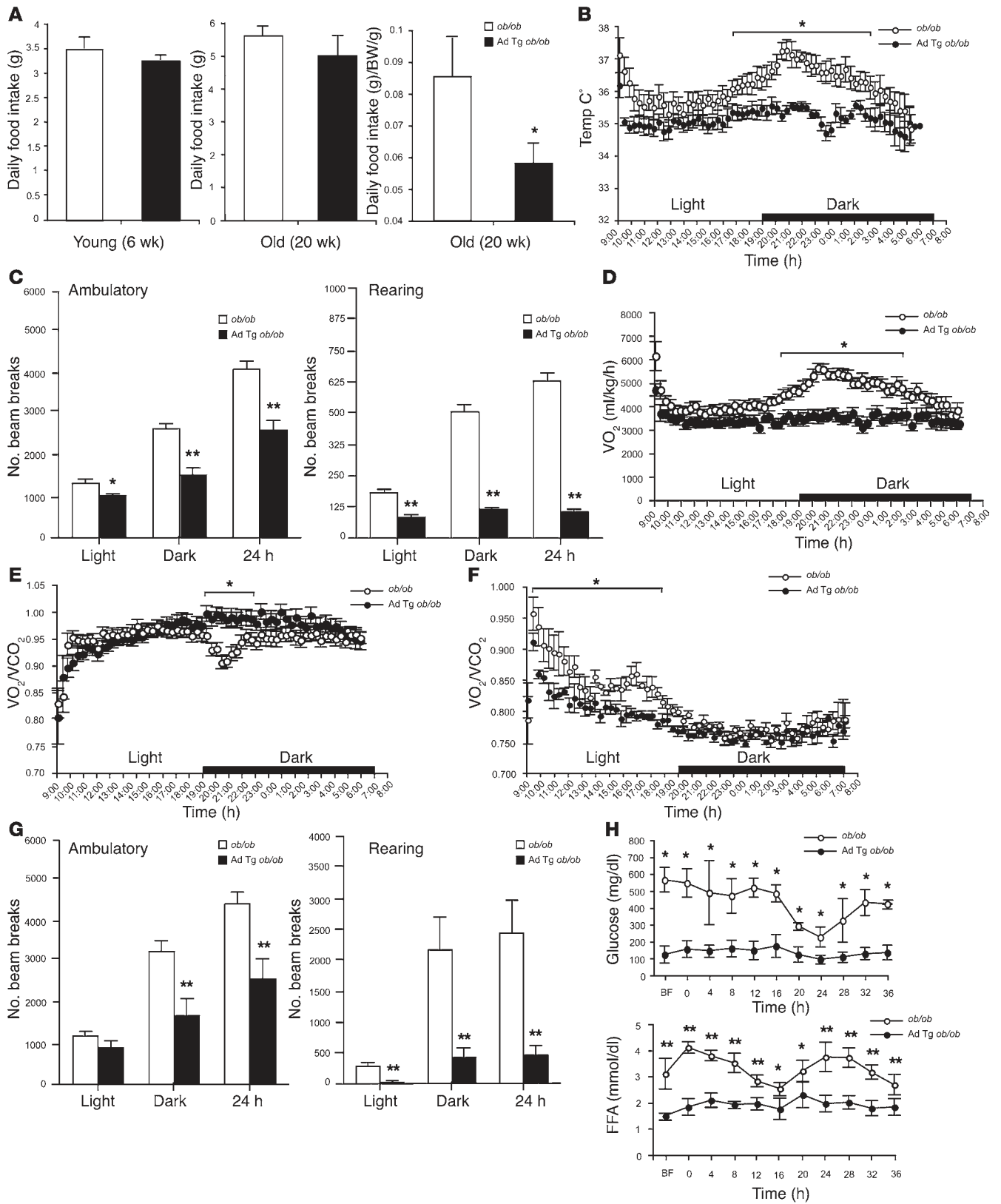




## Figure 6

Metabolic cage studies on adiponectin-expressing *ob/ob* mice and *ob/ob* littermates under normal and fasting conditions. (A) Daily food uptake was monitored at 6 weeks of age (left) and 20 weeks of age (middle and right) and represented in absolute amounts (left and middle) or expressed as food intake per total body weight (BW) (middle and right) in adiponectin transgenic *ob/ob* mice and *ob/ob* littermates ( $n = 3\text{--}5$  mice/group). (B) Core body temperature (temp.), (C) activity (ambulatory on the left, rearing on the right), (D)  $\text{VO}_2$ , and (E) RER were measured in adiponectin transgenic *ob/ob* mice and *ob/ob* littermates. ( $n = 3$  mice/group). Male adiponectin transgenic *ob/ob* mice and *ob/ob* littermates were denied access to food for 36 hours. (F) RER and (G) activity (ambulatory on the left, rearing on the right) were analyzed during the course of study. (H) Glucose (top) and FFAs (bottom). Blood was collected every 4 hours over a period of 36 hours to measure plasma glucose and FFAs. \* $P < 0.05$ ; \*\* $P < 0.01$ . For B–H, 12-week-old male mice were used. All data were analyzed by ANOVA. BF, before food removal.

nectin that carries a deletion within the collagenous domain of the protein, leading to the formation of a subset of mixed WT/mutant complexes. The detailed mechanism of action of these mutant protein complexes is currently under study in our laboratory. The net effect is an improved efficacy of the secretory pathway with respect to adiponectin assembly and release, leading to a 2- to 3-fold elevation of steady state levels of WT adiponectin complexes in plasma.

We challenged these mice metabolically by breeding them into the *ob/ob* background. The leptin deficiency induced hyperphagia. This resulted in a gradual increase in adipose tissue mass. Under these conditions, this expansion of the fat mass was associated with a reduction of circulating adiponectin levels. However, in the transgenic mice, this obesity-induced downregulation did not occur, but instead, there was a constitutive elevation of both intracellular and plasma adiponectin levels despite a continued increase in fat mass. The end result of this chronic elevation of adiponectin in transgenic *ob/ob* mice was a very significant expansion of the fat mass.

Phenotypically, this resulted in improvements in all metabolic parameters examined as they relate to glucose and lipid metabolism. Concomitant with the metabolic improvements, there was a positive impact on the inflammatory profile. The underlying mechanisms for these improvements are complex, but are likely related to the general increase in the local activity of PPAR $\gamma$  in adipocytes. Ultimately, this increased PPAR $\gamma$  activity in adipocytes resulted in a redistribution of lipids from ectopic deposits in liver and muscle to the subcutaneous adipose depots. As a result, hepatic insulin sensitivity increased, translating into systemic improvements in insulin sensitivity and preservation of  $\beta$  cell mass.

This suggests a role for adiponectin as a “starvation signal” released by the adipocytes, providing a systemic indication that the average adipocyte size is small and that adipose tissue is in need of accumulating higher levels of triglyceride. We have previously examined seasonal variations of adiponectin levels in yellow-bellied marmots and found that adiponectin levels are highest during the summer and fall months, a time when the marmots massively increase their fat stores (17). In addition, Froguel and colleagues recently identified a nucleotide polymorphism in the gene encoding adiponectin that is associated with severe forms of childhood obesity and, importantly, increased levels of adiponectin in the plasma of these children (18).

Adiponectin is consistently upregulated in the lean state with further elevation in anorexic states (19, 20) and correspondingly downregulated in overweight and obese states (21, 22). This type of regulation is a fundamentally different from the regulatory mechanism in place for leptin. Leptin levels tend to be directly proportional to fat mass and do not display the inverse relationship that adiponectin displays with adipose tissue mass (23). Generally, adiponectin and leptin are regulated in an opposite fashion under many different physiological states (24). Hence, elevated

adiponectin levels go hand in hand with low leptin levels and may send comparable systemic signals. As an example, we have previously reported that transgenic overexpression of adiponectin in WT mice (under normal conditions a reflection of limited systemic energy stores) causes infertility in females, a phenomenon that can also be triggered with low leptin levels (25).

Much excitement has been created by the original observation that obesity is associated with increased infiltration of macrophages into the growing fat pads. Several different models have been proposed to mechanistically explain why macrophages infiltrate obese fat pads with higher frequency. Monocyte chemoattractant protein-1 (MCP-1) and its receptor C-C motif chemokine receptor-2 (CCR2) have recently been implicated in this process (26, 27). MCP-1 is produced at higher levels in obese fat pads and hence attracts a higher number of macrophages (28). An alternative model has recently been proposed by Cinti and colleagues (29). These authors suggest that adipocytes that reach a maximal size upon lipid loading spontaneously undergo necrosis, which is associated with increased infiltration of macrophages around the dying adipocyte. Our massively obese mice do not allow us to differentiate between these 2 models. We report a reduction in both average adipocyte size and local inflammation. However, our transgenic line supports strongly the hypothesis that macrophage infiltration is not a function of absolute adipose tissue mass but rather relates to the “quality” of the individual fat cell in the adipose pad. Transgenic overexpression of adiponectin led to a massive expansion of adipose tissue mass, yet the level of macrophage infiltration was quite minimal, likely due to the fact that these mice showed hyperplasia but not hypertrophy. We conclude that macrophage infiltration is clearly not a function of adipose tissue quantity alone but rather a reflection of the quality of the individual adipocyte.

Adiponectin overexpression also has an impact on lipid levels. This is of interest in the context of *ob/ob* mice. In contrast with humans, HDL cholesterol levels are increased in genetic mouse models of obesity (*ob/ob* and *db/db*) (9, 30, 31) due to their decreased clearance rates (9, 32). The appearance of large apoE-rich HDL-1 particles in these animals suggested a normal lipodation process, thus implying that the decreased clearance can account for the increase in total HDL levels in *ob/ob* mice compared with WT mice (31). In the present study, adiponectin-overexpressing *ob/ob* mice exhibited significantly lower total plasma cholesterol levels than the *ob/ob* controls (data not shown). Gel filtration analysis of lipoprotein profiles show markedly decreased HDL-1 and HDL peaks. More importantly, the lipoprotein profiles of adiponectin-overexpressing *ob/ob* mice closely resemble the profiles of WT mice, suggesting that adiponectin normalizes HDL concentration and HDL particle size in *ob/ob* mice. The adiponectin-related effects on HDL levels are consistent with a general improvement seen for the lipid profiles in the context of rodent obesity. This is

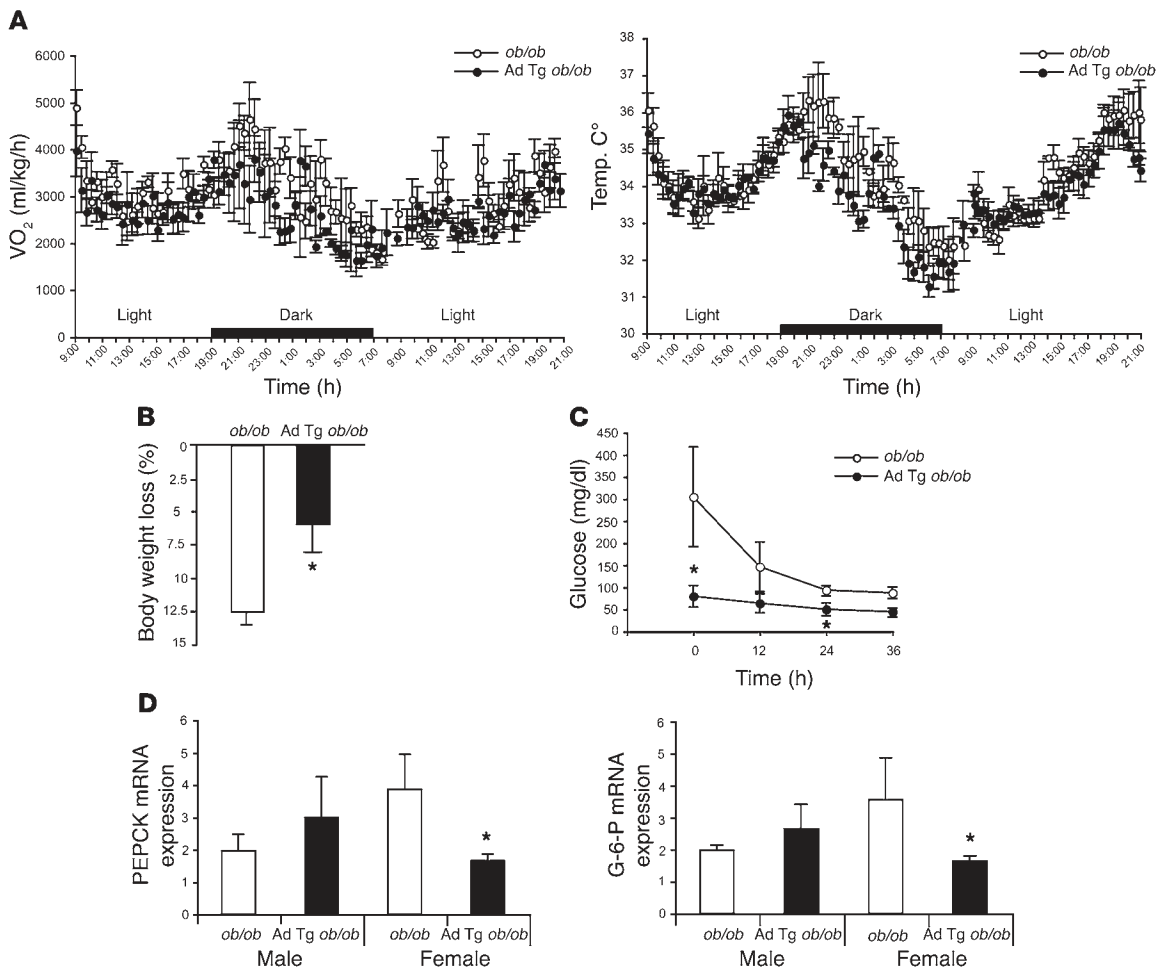


**Figure 7**

Pronounced hypoglycemia in female adiponectin transgenic *ob/ob* mice during fasting. In a separate experiment, female and male adiponectin transgenic *ob/ob* mice and *ob/ob* littermates were examined during a fast. (A) VO<sub>2</sub> (left) and core body temperature (right) were monitored in 12-week-old male mice. (B) Change of body weight over the fasting period in 12-week-old female mice is shown. (C) Glucose levels of 12-week-old females during a 36-hour fast is shown. (D) Mice were sacrificed after 36 hours of fasting, and liver tissue was collected. qRT-PCR for PEPCK and G-6-P was performed from RNA of liver (A–D; n = 3 mice/group). \*P < 0.05. All data were analyzed by ANOVA except panels A and D, which were analyzed by Student’s t test.

not a peculiarity of adiponectin overexpression in the *ob/ob* background, since we found that adiponectin overexpression also further reduces HDL-1 and HDL peaks in WT mice (our unpublished observations). This finding constitutes a novel observation that is consistent with the increased activity of LPL in adipose tissue of adiponectin-overexpressing mice. This is likely to be responsible for increased triglyceride clearance from circulation after an oral lipid challenge. Correspondingly, we demonstrate that triglyceride concentrations were decreased in the VLDL fractions in the presence of excess adiponectin.

The differences in HDL size and plasma concentrations also suggest a role for adiponectin in HDL metabolism. Although the detailed molecular mechanisms for the decrease in HDL cholesterol of adiponectin-overexpressing mice are not known, it is likely that HDL turnover is accelerated in adiponectin-overexpressing mice. Factors known to affect HDL turnover are under current investigation. Important differences in lipoprotein metabolism between humans and mice have to be taken into account though.

Epidemiological data suggest a strong correlation between HDL levels and adiponectin levels (33, 34). In light of this, the relationship of adiponectin overexpression to HDL-cholesterol levels and atherosclerosis in mice is paradoxical. While we see a marked reduction of HDL-cholesterol levels in this model of adipocyte-derived overexpression of adiponectin, hepatic overexpression of globular adiponectin reduces atherosclerosis and neointima formation after arterial injury (35, 36). These apparently contrasting findings may be due to the ability of adiponectin to facilitate reverse cholesterol transport. Previous studies with mice overexpressing scavenger receptor class B type 1 (SR-B1) in liver demonstrated marked increases in reverse cholesterol transport and significantly reduced HDL cholesterol levels (37) but resulted in reduction of atherosclerosis (38). Hence, this leads to a model of adiponectin action that promotes reverse cholesterol transport triggering beneficial effects on atherogenesis without raising HDL cholesterol levels. Furthermore, recent clinical studies also supported a strong correlation of plasma adiponectin levels with



plasma LPL activity and an inverse correlation with hepatic lipase activity independent of insulin resistance or inflammation (39, 40). Combined, our findings strongly support an integral role of adiponectin in lipoprotein metabolism beyond its well-known role in insulin sensitization (6, 41, 42).

To study the metabolic phenotype of the transgenic animals in more detail, we used calorimetric cages. Metabolic cage studies revealed that transgenic *ob/ob* mice were not hyperphagic compared with their *ob/ob* controls. In fact they ate much less when adjusted for total body weight. This is in contrast to what one would expect considering their obese phenotype and considering the fact that they lack leptin. The massive obesity may be unleashed because leptin and adiponectin exert antagonistic effects. Lack of one of these adipokines combined with overexpression of the other leads to the phenotype described here. We have previously shown that mice lacking functional leptin are hyperresponsive to an injection of recombinant adiponectin (41). Even though food intake was similar between both groups, there are clear metabolic differences. Core temperature as well as activity levels were considerably lower in transgenic *ob/ob* mice. The reduced activity levels could be explained in part by the massive obesity. Consistent with these observations, oxygen consumption was also decreased compared with controls. RER levels were similar overall. However, at the beginning of the dark period, RER levels were increased in transgenic mice, which may reflect increased carbohydrate utilization, which spared triglyceride oxidation and stimulated the accumulation of adipose tissue. To investigate whether the animals had problems switching from carbohydrate to fat utilization as a main source of energy, the animals underwent a longer-term and short-term metabolic challenge by fasting and by administration of central 2DG, respectively. In general, the transgenic animals showed an altered response to fasting, switching more rapidly to FFA-based metabolism. The transgenic mice lost considerably less weight upon food deprivation, an indication that they had difficulty dipping into their triglyceride stores during caloric deprivation. This was particularly apparent in female mice, which developed a more severe form of hypoglycemia than males. Consistent with that, mRNA levels encoding gluconeogenic enzymes such as PEPCK and G-6-P were reduced in the females, which displayed a significantly higher degree of adiponectin overexpression than the males (6). Nevertheless, the reduced body core temperature and reduced motility enabled both males and females to sustain glucose levels allowing them to survive the fast, despite the strong trend toward a metabolically inappropriate preservation of fat mass during times of starvation.

An additional striking observation was the total lack of diurnal rhythmicity of several metabolic parameters in the transgenic animals, which was restored to the level of *ob/ob* mice during an acute fast. These changes suggest that adiponectin interacts in an inhibitory fashion with circadian oscillators in multiple central and peripheral tissues involved in maintaining energy homeostasis (43).

While factors such as the maintenance of body core temperature, oxygen consumption, and locomotor activity are centrally regulated and were clearly altered in the transgenic mice, other aspects of central regulation of glucose homeostasis were normalized. Recent data has demonstrated the powerful effects of central hypothalamic regulation on hepatic glucose homeostasis (44–46). In the transgenic mice, these central regulatory mechanisms were restored to the level of WT controls. Central infusion of minute amounts of 2DG offered a powerful challenge, effectively mimicking acute

peripheral hypoglycemia. When performed in WT animals, this triggered release of glucose from the liver, a process which was effectively restored in the transgenic animals, while *ob/ob* animals failed to respond peripherally to this central starvation signal.

In summary, we have described a model of chronic overexpression of adiponectin that leads to a massive increase in subcutaneous fat mass and protection against diet-induced insulin resistance. We believe that this mouse model is an excellent preclinical model to study the effects of adipose tissue expansion in the subcutaneous region in patients as well. There is the well-appreciated fact that not all obese patients are insulin resistant. Even more dramatically, not all morbidly obese patients display insulin resistance, and an elevation of adiponectin levels is frequently associated with improved metabolic profiles (47). Hepatic steatosis is often associated with systemic insulin resistance (5). The mechanism of action of antidiabetic compounds such as PPAR $\gamma$  agonists heavily relies on the ability of these ligands to reduce hepatic lipid content associated with a concomitant increase in subcutaneous fat mass. In the context of PPAR $\gamma$  agonists, this effect critically depends on their ability to induce adiponectin (48, 49). Independently, Cooper and colleagues have demonstrated the potent anti-steatotic effects of adiponectin in the liver (50). Furthermore, our analysis here demonstrates the closely linked gene expression pattern in white adipocytes from adiponectin-overexpressing adipocytes with the transcriptional hallmarks seen for PPAR $\gamma$  agonist treatment in the same cells. This parallel between adiponectin overexpression and PPAR $\gamma$  agonist action warrants further study. There is a striking overlap between the 2 conditions. PPAR $\gamma$  activity is increased by adiponectin, and adiponectin increases PPAR $\gamma$  activity. This demonstrates for what we believe is the first time a remarkable feed-forward loop between adiponectin and PPAR $\gamma$ , which appears to be functional only when one or the other is constitutively stimulated (transgenic adiponectin overexpression or pharmacological PPAR $\gamma$  activation). Under more physiological conditions (e.g., intact *ob/ob* mice), this loop appears to be interrupted by unknown mechanisms.

All of these observations strongly suggest that adiponectin is a central player antagonizing the metabolic axis of evil involving obesity, hepatic lipid deposition, and local inflammation, leading ultimately to systemic insulin resistance. Therefore, the inability to sustain elevated adiponectin levels during times of excess caloric intake leads to reduced lipid deposition in the subcutaneous region, causing ectopic fat accumulation in liver and associated insulin resistance. Type 2 diabetes could therefore be viewed as a failure to appropriately expand fat mass in the context of a positive energy balance (51).

## Methods

**Animals.** All animal experimental protocols were approved by the Institute for Animal Studies of the Albert Einstein College of Medicine. Adiponectin transgenic *ob/ob* mice were generated by mating heterozygous leptin-deficient (*ob/+*) mice with adiponectin transgenic mice (6). Mice were housed in groups of 2–5 in filter-top cages. The colony was maintained in a pathogen-free Assessment and Accreditation of Laboratory Animal Care-accredited facility at the Albert Einstein College of Medicine under controlled environment settings (22–25°C, 40%–50% humidity). Mice were maintained on 12-hour light and dark cycles with ad libitum access to water and standard chow diet (5058; LabDiet) or high-fat diet (D12492; Research Diets Inc.) as indicated. All experiments presented were littermate controlled and were performed on a mixed C57BL/6 and FVB background. Many experiments



were repeated on a purer C57BL/6 background (backcross 6 and higher) with identical results. Results reported were generally seen in male and female mice unless specifically indicated.

**MRI and 3D reconstruction.** Frozen hearts with attached pericardial fat pads were transferred after thawing to a 16.6-mm diameter tube with agarose to prevent dehydration of the tissue. This tube was placed in a custom-built 38-mm inner diameter radio frequency (RF) coil (RF Sensors LLC Inc.). MRI images were acquired in 3 planes (transversal, coronal, and sagittal) with spin echo sequence at 11 °C in a GE Omega 9.4T vertical bore nuclear magnetic resonance (NMR) system (Fremont Inc.). Echo and repetition time values were 18 ms and 300 ms, respectively. After acquisition, images were exported and transformed to jpg format images in a custom-designed software that runs in the MATLAB (MathWorks Inc.). The images then were loaded into Amira (Mercury Computer Systems Inc.) sequentially as a single entity keeping the proper order, slice separation, field of view, and slice thickness. After this, the region of interest was selected and defined using label field function in Amira in the 3 planes. Finally, labeling of heart and pericardial fat tissues was performed, leading to the their 3D reconstruction.

**Assay protocols.** Serum values for glucose were measured by FastBlue B glucose assay (Sigma-Aldrich) and adiponectin with a mouse adiponectin RIA kit (Linco; Millipore). Insulin was measured with a mouse insulin RIA kit (Linco; Millipore). OGTTs were performed in animals without access to food for 2 hours prior to administration of 2.5 g/kg body weight glucose load by oral gavage and during the course of the study. Fasting glucose, insulin, triglycerides, and FFA levels were measured at 3 hours after mice were denied access to food. For fasting studies, blood was collected every 4 hours during 36 hours and used for glucose and FFA (NEFA C; Wako) measurements. For triglyceride clearance, mice were fasted for 3 hours and then weighed at 10 am and given 15  $\mu$ l of olive oil/g body weight by gastric gavage. Approximately 20  $\mu$ l of blood was collected at 0, 2, 4, 6, and 8 hours and assayed for triglyceride (Infinity Triglyceride Kit; Thermo Scientific). Mice were denied access to food during the course of the study.

**PPAR $\gamma$  agonist gavage and tissue collection.** The PPAR $\gamma$  agonist 2-(2-(4-phenoxy-2-propylphenoxy)ethyl)indole-5-acetic acid (COOH) was a kind gift from Merck (52). The COOH and vehicle were gavaged daily at 12 noon for 10 days at 10 mg/kg body weight. Mice were subjected to tail bleeding 4 hours after the last gavage, and 30  $\mu$ l serum was collected. Mice were then sacrificed within 6 hours after the last gavage, and adipose tissues were collected.

**Immunoblot analysis.** Protein extraction and Western blot from fat tissues were performed as previously described (6). For adipose tissues, materials were first put into TNET buffer (150 mM NaCl, 5 mM EDTA, 50 mM Tris-HCl, pH 7.5) without Triton X-100 and homogenized. After low-speed centrifugation (2,600 g at 4 °C), the fat cake was removed from the top of the tube, and Triton X-100 was added to a final concentration of 1%. After incubating at 4 °C for 30 minutes, the extract was cleared at 20,000 g for 15 minutes at 4 °C and mixed with 2 $\times$  Laemmli sample buffer. Protein samples were loaded on 10% Bis-Tris NuPAGE gels (1.5 mm; Invitrogen) for analysis with indicated antibodies. We analyzed 30  $\mu$ g of protein extract for adiponectin or guanosine diphosphate (GDP) dissociation inhibitor (GDI). The antibody against GDI was kindly provided by Perry Bickel (Washington University, St. Louis, Missouri, USA). Each band was detected and quantitated by the Odyssey Infrared Imaging System (LI-COR Biosciences).

**Immunohistochemistry for F4/80 marker.** Freshly isolated tissues were fixed with phosphate-buffered formalin overnight, then paraffin wax embedded and subsequently deparaffinized. Sections of 5  $\mu$ m were incubated overnight with a monoclonal anti-F4/80 antibody. After washing in PBS, slides were incubated with biotinylated goat anti-rat or anti-rat IgG at 5  $\mu$ g/ml (Vector Laboratories) for 1 hour at room temperature. Slides were developed using a peroxidase detection kit (Vector Laboratories) and counterstained with hematoxylin (Sigma-Aldrich).

**Immunofluorescence staining for insulin and glucagon.** Pancreas tissue was fixed in Bouin fixative (saturated picric acid: formaldehyde: glacial acetic acid at a ratio of 15:5:1) for 5 hours. Paraffin sections (5  $\mu$ m) were incubated with control donkey IgG (1:500; Jackson ImmunoResearch Laboratories Inc.) for 1 hour to block nonspecific binding. Sections were then incubated with guinea pig anti-mouse insulin antibody (1:500; a kind gift from Regina Kuliawat, Albert Einstein College of Medicine, New York, New York, USA) and rabbit anti-human glucagon antibody (1:500; Invitrogen) overnight at 4 °C. After washing with PBS 3 times, sections were incubated with FITC-conjugated donkey anti-guinea pig antibody and Texas red-conjugated donkey anti-rabbit antibody (1:250; Jackson ImmunoResearch Laboratories Inc.) for 1 hour at room temperature. Sections were analyzed with an Olympus IX81 microscope.

**Treatment of mice with monoclonal antibodies.** Mice were treated for 1 week with a mixture of monoclonal antibodies. Antibodies were previously described (53). We injected 50  $\mu$ g of a 1:1 mixture of the 2 monoclonal antibodies (or an equivalent amount of nonimmune mouse antibodies) i.p. on days 1, 4, and 7 of the experiment.

**In vivo insulin signaling.** Mice were food deprived for 6 hours and subjected to an i.p. injection of human recombinant insulin at 1 mU/g body weight. Mice were then sacrificed at various times; livers were isolated and snap frozen. Subsequently, liver tissues were lysed in radioimmunoprecipitation assay (RIPA) buffer (54), and immunoprecipitations were performed with anti-insulin receptor antibodies (Insulin R $\beta$ , sc-711; Santa Cruz Biotechnology Inc.) and analyzed by Western blot analysis, decorated with anti-phosphotyrosine clone 4G10 (Millipore). Alternatively, extracts were directly analyzed by Western blots using phospho-AKT (9271; Cell Signaling Technology Inc.), phospho-GSK3 $\beta$  (9336; Cell Signaling Technology Inc.), Akt-1 (c-20; Santa Cruz Biotechnology Inc.), and GSK3 $\beta$  (sc-7291; Santa Cruz Biotechnology Inc.). Results were analyzed by the Odyssey Infrared Imaging System (LI-COR Biosciences).

**Assessment of macrophage prevalence in adipose tissue stromal vascular fractions.** Adipose tissue from transgenic and *ob/ob* mice was subjected to collagenase digestion (1 mg collagenase/g adipose tissue) in Krebs-Ringer bicarbonate buffer (KRB) containing 4% fatty-acid-poor BSA and 1  $\mu$ M adenosine at 37 °C for 1 hour. Cell digestion was strained using a 200- $\mu$ m mesh filter, and the resulting free adipocytes and stromal vascular cells (SVCs) were subjected to brief centrifugation at 500 g for 1 minute. The infranant containing the SVCs was removed and centrifuged for 5 minutes at 500 g. The SVC pellet was washed 2 times in KRB, then incubated in erythrocyte lysis buffer, pH 7.3, for 10 minutes at room temperature. Remaining SVCs were washed 2 times in ice-cold FACS buffer (PBS containing 5 mM EDTA and 0.2% fatty-acid-poor BSA). Cells were counted using a hemocytometer, and aliquots of 10<sup>6</sup> cells were prepared for analysis. Cells were incubated for 30 minutes in 1 ml FACS buffer containing FcBlock (20  $\mu$ g/ml; BD), then with FITC-conjugated anti-F4/80 IgG (5  $\mu$ g/ml) for 1 hour at 4 °C. F4/80 positive cells were detected using FACScan (BD), and analysis was performed using CellQuest software (BD).

**Analysis of adiponectin complex distribution.** The complex distribution of adiponectin was determined by separating 15  $\mu$ l of mouse serum over a Superdex 200 10/300 GL column (GE Healthcare) using a BioLogic Workstation fast-performance liquid chromatography (FPLC) system (Bio-Rad). The column was equilibrated in column buffer (25 mM HEPES, pH 8.0, 150 mM NaCl, 1 mM CaCl<sub>2</sub>), and 0.22 ml fractions were collected. Samples (40  $\mu$ l) were collected over the entire elution of adiponectin and incubated with 10  $\mu$ l of 5 $\times$  Laemmli sample buffer followed by boiling for 5 minutes. Samples were loaded on a Criterion precast 26-well gel (Bio-Rad) and subjected to immunoblotting using 1:500 polyclonal anti-adiponectin antibody followed by incubation with IRDye 800-coupled



goat anti-rabbit secondary antibody (Rockland Immunochemicals). The fluorescence signal obtained at 30 kDa was quantitated by the Odyssey Infrared Imaging System (LI-COR Biosciences).

**RNA isolation and analysis.** RNA was isolated from frozen fat tissue by using QIAGEN RNeasy tissue kit following the manufacturer's protocol. cDNA was synthesized from isolated RNA using SuperScript II and oligo dT (Invitrogen). Quantitative PCR was performed with the LightCycler-fast start master SYBER green (Roche Diagnostics) with the following primer sets: GAPDH (forward: 5'-AACTTTGGCATTGTGGAAGG-3', reverse: 5'-ACACATTGGGGGTAGGAACA-3'); F4/80 (forward: 5'-CTTTGGC-TATGGGCTCCAGTC-3', reverse: 5'-GCAAGGAGGACAGAGTTATC-GTG-3'); VCAM (forward: 5'-ATTTTCTGGGGCAGGAAGTT-3', reverse: 5'-ACGTCAGAACAACCGAATCC-3'); vWF (forward: 5'-TGCTTCTTAC-GCCCATCTCT-3', reverse: 5'-CAGCTGCCTTCCAGAAAAC-3'); PEPCK (2 primer sets were used interchangeably) (forward: 5'-AGCCTCGA-CAGCCTGCCCCAGG-3', reverse: 5'-CCAGTTGTTGACCAAAGCCTTTT-3'); (forward: 5'-CGATGACATCGCCTGGATGA-3', reverse: 5'-TCTTGCCCTTGTGTTCTGCA-3'); G-6-P (forward: 5'-GAAGGC-CAAGAGATGGTGTGA-3', reverse: 5'-TGCAGCTCTTGCAGTACATG-3'); aP2 (forward: 5'-GACGACAGGAAGGTGAAGAG-3', reverse: 5'-ACATTC-CACCACCAGCTTGT-3'); DGAT-1 (forward: 5'-GGCCTGCCCCATGC-GTGATTAT-3', reverse: (5'-CCCCACTGACCTTCTTCCCTGTAGA-3')); PPAR $\gamma$ 2 (forward: 5'-ACTGCCTATGACCACTTCCAC-3', reverse: 5'-CAATCGGATGGTTCTTCGGA-3'); TNF- $\alpha$  (forward: 5'-GAGAAAGT-CAACTCCTCTCTG-3', reverse: 5'-GAAGACTCCTCCAGGTATATG-3'). Each PCR reaction was normalized to  $\beta$ -actin (forward: 5'-TACCACAG-GCATTTGTGATGG-3', reverse: 5'-TTTGATGTCACGCAGATT-3').

**IL-6 measurements.** The serum IL-6 levels were determined by a mouse IL-6 immunoassay (Quantikine; R&D systems). The assay was performed according to the manufacturer's protocol.

**Body composition analysis.** Body composition was measured by MRI using an EchoMRI (Echo Medical Systems).

**Oil red O staining.** Frozen liver tissue sections were rinsed in water and placed in absolute propylene glycol for 2 minutes, then in oil red O solution. After 2 days, slides were transferred to an 85% propylene glycol solution for 1 minute for differentiation and counterstained with hematoxylin.

**Liver triglyceride and DAG measurements.** Frozen liver tissues (200 mg) were pulverized and transferred into 30 ml of chloroform/methanol solution (2:1). Samples were set at room temperature for 20 minutes and 6 ml of 0.05% H<sub>2</sub>SO<sub>4</sub> was added, followed by centrifugation at 2,000 g for 10 minutes at 4°C. Meanwhile, standards were prepared by serial dilution from 200  $\mu$ g Wesson oil (ConAgra Foods)/ml chloroform. For each standard and sample, 2 ml was transferred into glass tubes and mixed with 2 ml of 1% Triton X-100/chloroform. Samples were dried under nitrogen gas and reconstituted with water. Concentration of triglycerides of final samples were determined by Trig/GB (Roche Diagnostics) (55).

DAGs and ceramides were extracted from frozen tissue (~100 mg) with chloroform/methanol (2:1, v/v) containing 0.01% butylated hydroxytoluene. Prior to the extraction, known amounts of 1,3-dipentadecanoin, triheptadecanoin, and hexanoylsphingosine were added as internal standards. Extracted samples were evaporated to dryness and redissolved in 1 ml of hexane-methylene chloride-ethyl ether (95:5:0.5, v/v/v). DAGs were isolated from triglycerides by use of a diol-bonded phase SPE column (Waters) under vacuum, as described previously (56). In brief, the SPE column was preconditioned with 4 ml of hexane. Lipid extract was then placed on the column, and triglycerides were eluted with 8 ml of hexane-methylene chloride-ethyl ether (89:10:1, v/v/v). DAGs were eluted with 8 ml of hexane-ethyl acetate (85:15, v/v) into a second set of collection tubes. Solvent was evaporated to dryness under vacuum and redissolved in 0.5 ml of hexane-ethyl acetate (85:15, v/v) for liquid chromatography/

tandem mass spectrometry (LC/MS/MS) analysis. Monitoring for the presence of triheptadecanoin in the DAG fraction assessed the separation of triglycerides from DAGs.

**Lipoprotein analysis.** For lipoprotein separation, samples were pooled (0.2 ml) from 5 mice per group. The pooled plasma from each group was subjected to FPLC gel filtration on 2 Superose 6 columns (GE Healthcare) in series. The eluate was collected in 0.5 ml fractions at a flow rate of 0.5 ml/minute. Forty-seven fractions were collected, and total triglycerides and cholesterol levels of each fraction were determined using the Infinity Triglyceride and Cholesterol Kit (Thermo Electron Corp). For apo determination, same volumes of fractions 19 to 36 were used to perform immunoblot analysis with anti-apoE, -apoA1, and -apoA2 antibodies (Santa Cruz Biotechnology Inc.) using the Odyssey Infrared Imaging System (LI-COR Biosciences).

**Measurement of tissue LPL activity.** LPL enzyme activity assays in adipose tissue were performed as previously described (57). In brief, tissue homogenates were incubated with a substrate mixture containing [carboxyl-<sup>14</sup>C] triolein, and NEFAs released by LPL were separated and counted. LPL activity was expressed as microunits (1  $\mu$ U = 1  $\mu$ mol NEFA released per hour of incubation at 28°C). To account for genotype-related differences in tissue triglyceride content, data are expressed as LPL activity per gram of total tissue protein. Postheparin LPL activity was measured in plasma obtained 10 minutes after heparin injection (60 IU/kg) under conditions that inhibit hepatic lipase activity (58).

**Indirect calorimetry.** Prior to data collection, animals were implanted with E-mitters (Mini Mitter) under ketamine/xylazine anesthesia for temperature measurements and allowed 4 days for recovery. Animals were individually housed in metabolic chambers maintained at 20–22°C on a 12-hour light/12 dark cycle with lights on at 7 am. Metabolic measurements (oxygen consumption, food intake, locomotor activity, and core temperature) were obtained continuously using a CLAMS (Columbus Instruments) open-circuit indirect calorimetry system. Mice were provided with 35% fat nutritionally complete powdered diet (Research Diets Inc.) and tap water ad libitum, unless mentioned otherwise. Presented results contain data collected over at least 7 days following at least 2–4 days of adaptation to the metabolic cages.

**2DG infusions.** Response to brain injections of the acute metabolic stressor 2DG was studied in order to investigate how mice respond to an acute interruption of central glucose availability. To this end, all animals were implanted with a 23-gauge stainless steel cannula aimed at the third cerebral ventricle (i.c.v.; 0.3 mm posterior to bregma, 3 mm ventral to skull surface) under ketamine/xylazine anesthesia. After 4 days recovery, animals were injected with 0.1 mg in 1  $\mu$ l 2DG (Sigma-Aldrich) dissolved in artificial cerebrospinal fluid (Harvard Apparatus). Tail blood samples were taken at 0, 15, 30, 60, 90, and 120 minutes for the measurement of glucose levels.

**NimbleGen expression arrays: RNA purification and cRNA probe labeling.** Gonadal fat samples were frozen immediately in liquid nitrogen and transferred to a -80°C freezer until further processing. Total RNA was isolated using TRIzol reagent (Invitrogen). Additional purification of total RNA was achieved with an RNeasy Mini kit (QIAGEN). Total RNA samples had an absorbance ratio (A<sub>260</sub>/A<sub>280</sub>) of 1.97–2.00. The integrity of extracted RNAs was checked on denaturing agarose gels. From each sample, 10  $\mu$ g of total RNA was utilized to synthesize double-stranded cDNA using a SuperScript Double-Stranded cDNA Synthesis Kit (Invitrogen) and an oligo dT primer containing a T7 RNA polymerase promoter sequence (5'-GGCCAGTGAATTGTAATACGACTCACTATAGGGAGGGAGGCG-GTTTTTTTTTTTTTTTTTTTTTTT-3'; Invitrogen). The double-stranded cDNA samples were sent to NimbleGen Systems Inc. for cRNA synthesis, probe labeling, and microarray hybridization, as previously described (59).

**NimbleGen expression arrays: microarray hybridization and data collection.** We used a mouse gene expression array manufactured by NimbleGen Systems Inc. A dual-color hybridization strategy was used in this study, i.e., cRNA



probes from both control and transgene samples were labeled with either fluorescent cyanine 3 (Cy3) or cyanine 5 (Cy5), then both the Cy3- and Cy5-labeled probes were mixed and applied to 1 array slide. The hybridizations were performed on 3 independent microarrays. Microarray slides were scanned, and raw data and normalized gene cells were analyzed by NimbleGen NimbleGen Systems Inc. The ratio of Cy3 to Cy5 for each feature was calculated from all normalized data. Final values were taken from the average of 3 slides and were log transformed for statistical analysis.

**Statistics.** Results are shown as mean ± SEM. For studies shown in Figure 3, comparisons between genotypes for body weight and body weight gain were performed by 2-way (body weight) or 3-way (body weight gain) repeated measures ANOVA, with genotype, time, and (for body weight gain) diet as factors. For studies shown in Figures 6 and 7, including core temperature, indirect calorimetry, food intake, FFA, and glucose, comparisons between groups were performed by 2-way repeated measures ANOVA, with genotype and time as factors. For each dependent measure from the metabolic cage (RER, VO<sub>2</sub>, temperature, and food intake), primary data were considered as the average for each animal for each time point over 3 consecutive days, beginning after a 2- to 3-day adaptation period to the metabolic chambers. Post hoc comparisons were made using Neuman-Keuls tests. For all 24-hour time point comparisons in Figures 6 and 7, unpaired Student's *t* tests were performed. Differences were deemed significant at *P* ≤ 0.05.

Statistical analysis was performed by Student's *t* test with SigmaPlot 9.0 and ANOVA analysis with SigmaStat 2.0 (Systat). Significance was accepted at *P* < 0.05.

**Acknowledgments**

We thank members of the Scherer laboratory for helpful comments, in particular Zhao V. Wang for technical advice for immunofluorescence staining and Nils Hallberg for help in sta-

tistical analysis. Furthermore, we would like to thank our Albert Einstein College of Medicine (AECOM) Diabetes Research and Training Center (DRTC) Radioimmunoprecipitation Assay (RIA) Core Facility (Manju Surana) and the AECOM Cancer Center Hybridoma Facility (Susan Buhl) for their help as well as the AECOM Institute for Animal Studies under the direction of Larry Herbst and the AECOM Transgenic Core for their expert assistance. Lipoprotein analysis was performed in the Cardiovascular Core Laboratory of the Cincinnati Mouse Metabolic Phenotype Center, supported by NIDDK (DK59630). This work was supported by NIH grants R01-DK55758, R24-DK071030-01, R01-CA112023, and R21-DK075887 (to P.E. Scherer); R01-DK066618 (to G.J. Schwartz), the New York Obesity Research Center (NIH DK026687); and the Skirball Institute for Nutrient Sensing (to G.J. Schwartz and P.E. Scherer). P.E. Scherer is also a recipient of an Irma T. Hirsch Career Scientist Award. M.E. Trujillo is supported by a mentor-based postdoctoral fellowship award from the American Diabetes Association (7-05-MI-09). T. Schraw is supported by a postdoctoral fellowship from the American Heart Association (Heritage Foundation; 0625998T). S.M. Hofmann is supported by a Scientist Development Grant from the American Heart Association (AHA 0635079N).

Received for publication November 21, 2006, and accepted in revised form May 31, 2007.

Address correspondence to: Philipp E. Scherer, Touchstone Diabetes Center, Department of Internal Medicine, University of Texas Southwestern Medical Center, 5323 Harry Hines Blvd., Dallas, Texas 75390-9077, USA. Phone: (214) 648-8715; Fax: (214) 648-8720; E-mail: philipp.scherer@utsouthwestern.edu.

1. Scherer, P.E. 2006. Adipose tissue: from lipid storage compartment to endocrine organ. *Diabetes*. **55**:1537–1545.
2. Moitra, J., et al. 1998. Life without white fat: a transgenic mouse. *Genes Dev*. **12**:3168–3181.
3. Shimomura, I., et al. 1998. Insulin resistance and diabetes mellitus in transgenic mice expressing nuclear SREBP-1c in adipose tissue: model for congenital generalized lipodystrophy. *Genes Dev*. **12**:3182–3194.
4. Pajvani, U.B., et al. 2005. Fat apoptosis through targeted activation of caspase 8: a new mouse model of inducible and reversible lipodystrophy. *Nat. Med*. **11**:797–803.
5. Yki-Jarvinen, H. 2005. Fat in the liver and insulin resistance. *Ann. Med*. **37**:347–356.
6. Combs, T.P., et al. 2004. A transgenic mouse with a deletion in the collagenous domain of adiponectin displays elevated circulating adiponectin and improved insulin sensitivity. *Endocrinology*. **145**:367–383.
7. Combs, T.P., et al. 2003. Sexual differentiation, pregnancy, calorie restriction, and aging affect the adipocyte-specific secretory protein adiponectin. *Diabetes*. **52**:268–276.
8. Gruijic, D., et al. 1997. Beta3-adrenergic receptors on white and brown adipocytes mediate beta3-selective agonist-induced effects on energy expenditure, insulin secretion, and food intake. *J. Biol. Chem*. **272**:17686–17693.
9. Silver, D.L., Jiang, X.C., and Tall, A.R. 1999. Increased high density lipoprotein (HDL), defective hepatic catabolism of ApoA-I and ApoA-II, and decreased ApoA-I mRNA in ob/ob mice. Possible role of leptin in stimulation of HDL turnover. *J. Biol. Chem*. **274**:4140–4146.
10. Molina, P.E., et al. 1993. Hormonal and metabolic effects of neuroglucopenia. *Brain Res*. **614**:99–108.
11. Yu, C., et al. 2002. Mechanism by which fatty acids inhibit insulin activation of insulin receptor substrate-1 (IRS-1)-associated phosphatidylinositol 3-kinase activity in muscle. *J. Biol. Chem*. **277**:50230–50236.
12. Samuel, V.T., et al. 2004. Mechanism of hepatic insulin resistance in non-alcoholic fatty liver disease. *J. Biol. Chem*. **279**:32345–32353.
13. Neschen, S., et al. 2005. Prevention of hepatic steatosis and hepatic insulin resistance in mitochondrial acyl-CoA:glycerol-sn-3-phosphate acyltransferase 1 knockout mice. *Cell Metab*. **2**:55–65.
14. Savage, D.B., et al. 2006. Reversal of diet-induced hepatic steatosis and hepatic insulin resistance by antisense oligonucleotide inhibitors of acetyl-CoA carboxylases 1 and 2. *J. Clin. Invest*. **116**:817–824. doi:10.1172/JCI27300.
15. Weisberg, S.P., et al. 2003. Obesity is associated with macrophage accumulation in adipose tissue. *J. Clin. Invest*. **112**:1796–1808. doi:10.1172/JCI200319246.
16. Nawrocki, A.R., and Scherer, P.E. 2005. Keynote review: the adipocyte as a drug discovery target. *Drug Discov. Today*. **10**:1219–1230.
17. Florant, G.L., et al. 2004. Fat-cell mass, serum leptin and adiponectin changes during weight gain and loss in yellow-bellied marmosets (*Marmota flaviventris*). *J. Comp. Physiol. B* **174**:633–639.
18. Bouatia-Naji, N., et al. 2006. ACDC/adiponectin polymorphisms are associated with severe childhood and adult obesity. *Diabetes*. **55**:545–550.
19. Delporte, M.L., Brichard, S.M., Hermans, M.P., Beguin, C., and Lambert, M. 2003. Hyperadiponectinaemia in anorexia nervosa. *Clin. Endocrinol. (Oxf)*. **58**:22–29.
20. Brichard, S.M., Delporte, M.L., and Lambert, M. 2003. Adipocytokines in anorexia nervosa: a review focusing on leptin and adiponectin. *Horm. Metab. Res*. **35**:337–342.
21. Arita, Y., et al. 1999. Paradoxical decrease of an adipose-specific protein, adiponectin, in obesity. *Biochem. Biophys. Res. Commun*. **257**:79–83.
22. Weyer, C., et al. 2001. Hypoadiponectinemia in obesity and type 2 diabetes: close association with insulin resistance and hyperinsulinemia. *J. Clin. Endocrinol. Metab*. **86**:1930–1935.
23. Frederich, R.C., et al. 1995. Expression of ob mRNA and its encoded protein in rodents. Impact of nutrition and obesity. *J. Clin. Invest*. **96**:1658–1663.
24. Matsubara, M., Maruoka, S., and Katayose, S. 2002. Inverse relationship between plasma adiponectin and leptin concentrations in normal-weight and obese women. *Eur. J. Endocrinol*. **147**:173–180.
25. Messinis, I.E., and Milingos, S.D. 1999. Leptin in human reproduction. *Hum. Reprod. Update*. **5**:52–63.
26. Weisberg, S.P., et al. 2006. CCR2 modulates inflammatory and metabolic effects of high-fat feeding. *J. Clin. Invest*. **116**:115–124. doi:10.1172/JCI24335.
27. Kanda, H., et al. 2006. MCP-1 contributes to macrophage infiltration into adipose tissue, insulin resistance, and hepatic steatosis in obesity. *J. Clin. Invest*. **116**:1494–1505. doi:10.1172/JCI26498.
28. Sartipy, P., and Loskutoff, D.J. 2003. Monocyte chemoattractant protein 1 in obesity and insulin resistance. *Proc. Natl. Acad. Sci. U. S. A.* **100**:7265–7270.
29. Cinti, S., et al. 2005. Adipocyte death defines macrophage localization and function in adipose tissue of obese mice and humans. *J. Lipid Res*. **46**:2347–2355.
30. Lundasen, T., Liao, W., Angelin, B., and Rudling, M. 2003. Leptin induces the hepatic high density lipoprotein receptor scavenger receptor B type I (SR-BI) but not cholesterol 7alpha-hydroxylase





- (Cyp7a1) in leptin-deficient (ob/ob) mice. *J. Biol. Chem.* **278**:43224–43228.
31. Gruen, M.L., et al. 2005. Persistence of high density lipoprotein particles in obese mice lacking apolipoprotein A-I. *J. Lipid Res.* **46**:2007–2014.
  32. Silver, D.L., Wang, N., and Tall, A.R. 2000. Defective HDL particle uptake in ob/ob hepatocytes causes decreased recycling, degradation, and selective lipid uptake. *J. Clin. Invest.* **105**:151–159.
  33. Yamamoto, Y., et al. 2002. Correlation of the adipocyte-derived protein adiponectin with insulin resistance index and serum high-density lipoprotein-cholesterol, independent of body mass index, in the Japanese population. *Clin. Sci.* **103**:137–142.
  34. Lara-Castro, C., Luo, N., Wallace, P., Klein, R.L., and Garvey, W.T. 2006. Adiponectin multimeric complexes and the metabolic syndrome trait cluster. *Diabetes.* **55**:249–259.
  35. Matsuda, M., et al. 2002. Role of adiponectin in preventing vascular stenosis. The missing link of adipo-vascular axis. *J. Biol. Chem.* **277**:37487–37491.
  36. Yamauchi, T., et al. 2003. Globular adiponectin protected ob/ob mice from diabetes and apoE deficient mice from atherosclerosis. *J. Biol. Chem.* **278**:2461–2468.
  37. Zhang, Y., et al. 2005. Hepatic expression of scavenger receptor class B type I (SR-BI) is a positive regulator of macrophage reverse cholesterol transport in vivo. *J. Clin. Invest.* **115**:2870–2874. doi:10.1172/JCI25327.
  38. Arai, T., Wang, N., Bezouevski, M., Welch, C., and Tall, A.R. 1999. Decreased atherosclerosis in heterozygous low density lipoprotein receptor-deficient mice expressing the scavenger receptor BI transgene. *J. Biol. Chem.* **274**:2366–2371.
  39. von Eynatten, M., et al. 2004. Decreased plasma lipoprotein lipase in hypo adiponectinemia: an association independent of systemic inflammation and insulin resistance. *Diabetes Care.* **27**:2925–2929.
  40. Bobbert, T., et al. 2005. Changes of adiponectin oligomer composition by moderate weight reduction. *Diabetes.* **54**:2712–2719.
  41. Berg, A.H., Combs, T., Du, X., Brownlee, M., and Scherer, P.E. 2001. The adipocyte-secreted protein Acrp30 enhances hepatic insulin action. *Nat. Med.* **7**:947–953.
  42. Pajvani, U.B., et al. 2004. Complex distribution, not absolute amount of adiponectin, correlates with thiazolidinedione-mediated improvement in insulin sensitivity. *J. Biol. Chem.* **279**:12152–12162.
  43. Damiola, F., et al. 2000. Restricted feeding uncouples circadian oscillators in peripheral tissues from the central pacemaker in the suprachiasmatic nucleus. *Genes Dev.* **14**:2950–2961.
  44. Pocai, A., et al. 2005. Hypothalamic K(ATP) channels control hepatic glucose production. *Nature.* **434**:1026–1031.
  45. Pocai, A., Obici, S., Schwartz, G.J., and Rossetti, L. 2005. A brain-liver circuit regulates glucose homeostasis. *Cell Metab.* **1**:53–61.
  46. Lam, T.K., Gutierrez-Juarez, R., Pocai, A., and Rossetti, L. 2005. Regulation of blood glucose by hypothalamic pyruvate metabolism. *Science.* **309**:943–947.
  47. Cote, M., et al. 2005. Adiponectinemia in visceral obesity: impact on glucose tolerance and plasma lipoprotein and lipid levels in men. *J. Clin. Endocrinol. Metab.* **90**:1434–1439.
  48. Nawrocki, A.R., et al. 2006. Mice lacking adiponectin show decreased hepatic insulin sensitivity and reduced responsiveness to peroxisome proliferator-activated receptor gamma agonists. *J. Biol. Chem.* **281**:2654–2660.
  49. Kubota, N., et al. 2006. Pioglitazone ameliorates insulin resistance and diabetes by both adiponectin-dependent and -independent pathways. *J. Biol. Chem.* **281**:8748–8755.
  50. Xu, A., et al. 2003. The fat-derived hormone adiponectin alleviates alcoholic and nonalcoholic fatty liver diseases in mice. *J. Clin. Invest.* **112**:91–100. doi:10.1172/JCI200317797.
  51. Ailhaud, G., and Reach, G. 2001. Does obesity protect against diabetes? A new controversy [In French]. *Ann. Endocrinol. (Paris)*. **62**:S43–S54.
  52. Carley, A.N., et al. 2004. Treatment of type 2 diabetic db/db mice with a novel PPARgamma agonist improves cardiac metabolism but not contractile function. *Am. J. Physiol. Endocrinol. Metab.* **286**:E449–E455.
  53. Wang, Z.V., et al. 2007. Secretion of the adipocyte-specific secretory protein adiponectin critically depends on thiol-mediated protein retention. *Mol. Cell. Biol.* **27**:3716–3731.
  54. Cohen, A.W., Combs, T.P., Scherer, P.E., and Lisanti, M.P. 2003. Role of caveolin and caveolae in insulin signaling and diabetes. *Am. J. Physiol. Endocrinol. Metab.* **285**:E1151–E1160.
  55. Carr, T.P., Andresen, C.J., and Rudel, L.L. 1993. Enzymatic determination of triglyceride, free cholesterol, and total cholesterol in tissue lipid extracts. *Clin. Biochem.* **26**:39–42.
  56. Pacheco, Y.M., Perez-Camino, M.C., Cert, A., Montero, E., and Ruiz-Gutierrez, V. 1998. Determination of the molecular species composition of diacylglycerols in human adipose tissue by solid-phase extraction and gas chromatography on a polar phase. *J. Chromatogr. B Biomed. Sci. Appl.* **714**:127–132.
  57. Laplante, M., et al. 2003. PPAR-gamma activation mediates adipose depot-specific effects on gene expression and lipoprotein lipase activity: mechanisms for modulation of postprandial lipemia and differential adipose accretion. *Diabetes.* **52**:291–299.
  58. Watson, T.D., et al. 1995. Measurement and physiological significance of lipoprotein and hepatic lipase activities in preheparin plasma. *Clin. Chem.* **41**:405–412.
  59. Nuwaysir, E.F., et al. 2002. Gene expression analysis using oligonucleotide arrays produced by maskless photolithography. *Genome Res.* **12**:1749–1755.